Investigation of Reagent Delivery Formats and Implications for Higher-sensitivity Detection in Paper-based Diagnostics

Tinny Liang

A thesis submitted in partial fulfillment of

the requirements for the degree of

Master of Science

University of Washington

2014

Committee:

Elain Fu

Wendy Thomas

Program Authorized to Offer Degree:

Bioengineering

University of Washington

ABSTRACT

Investigation of Reagent Delivery Formats and Implications for Higher-sensitivity Detection in Paper-based Diagnostics

Tinny Liang

Chair of Supervisory Committee
Affiliate Assistant Professor Elain Fu
Bioengineering

Millions of people in developing countries die from infectious diseases (e.g. malaria), yet many of these deaths can be prevented if given the tools for accurate diagnosis. Current diagnostic capabilities with the required clinical sensitivity are confined to laboratory settings due to cost, electrical, and personnel requirements. Current POC diagnostics targeting infectious diseases in low resource settings, lateral flow tests (LFTs), have the appropriate usability, but are confined to a single chemical step, and as a result lack the required sensitivity for clinical utility. A two-dimensional paper network (2DPN) is an inexpensive new technology based on the strengths of LFTs but allows complex chemical processes to be performed. Fluid control tools are essential for the success of a 2DPN in carrying out complex chemical processes in an automated fashion. Three versions of a 2DPN-based amplified assay in a malaria detection system are demonstrated using three fluid control tools: paper network geometry, dissolvable sucrose barriers, and cellulose-based delay shunts. Using the same system, assays based on two delivery formats, sequential delivery of analyte and colorimetric label and premixed one step delivery were characterized for reproducibility, sensitivity, and time to result. The sequential delivery format offers the potential for higher sensitivity detection compared to the premix delivery format used by conventional LFTs, but at the expense of additional time to result. Next steps for implementation of a high-sensitivity 2DPN using the sequential format are discussed.

Table of Contents

Acknowledgements

This research was conducted at the University of Washington in the Department of Bioengineering, advised by Elain Fu. Elain's guidance was essential to the completion of this work. I would like to acknowledge my committee member, Wendy Thomas, for support and suggestions throughout the process. Additionally, it would not have been possible without the continued support and contributions of many other individuals. Jared Houghtaling was a valuable collaborator and friend throughout all of the research, especially with respect to the two-dimensional network demonstrations presented in Chapter 3. Paolo Spicar-Mihalic's initial work on optimizing the membrane cutting procedure was essential for the fabrication techniques described in Chapter 3. Barry Lutz's initial work on sucrose deposits on paper motivated the work on sucrose barriers presented in Chapter 3. Bhushan Toley and Brittney Mckenzie developed and characterized the pad-based shunts described in Chapter 3. The original Matlab analysis script was written by Stephen Ramsey. Peter Kauffman was invaluable in all optical, mechanical, and electronic needs.

The concepts and inspirations for this work came from discussion with all members of the Fu, Lutz, and Yager groups, specifically: Barry Lutz, Paul Yager, Jared Houghtaling, Gina Fridley, Carly Holstein, Sujatha Ramachandran, Josh Buser, Samantha Brynes, Bhushan Toley, Brittney Mckenzie, Greg Thiessen, Melissa Li, and Peter Kauffman.

This work is supported by funding from the National Science Foundation Graduate Research Fellowship under Grant No. DGE-1256082.

Chapter 1: Introduction

1.1 Significance

Malaria, human immunodeficiency virus (HIV), and tuberculosis (TB) are the three biggest causes of infectious disease burden in the developing world [1]. More than 50 % of the deaths in the poorest countries result from infectious diseases [2]. Neglected diseases combined affect over one billion people worldwide according to the World Health Organization (WHO) [3]. Approximately two million deaths per year are attributed to malaria infection. About 60 percent of these deaths are in children under the age of five [1, 4]. A disproportionate number of these deaths occur in Africa (Figure 1).

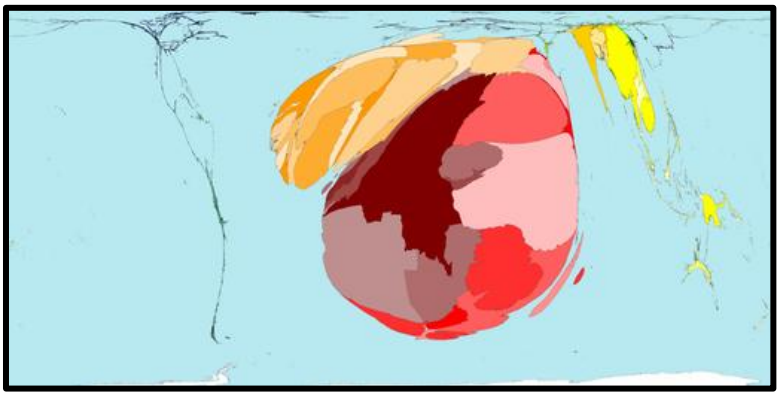

Figure 1. World map scaled to the proportion of global deaths from malaria that occurs in that region. A disproportionate number of deaths from malaria occur on the African continent [5].

Unfortunately many of these deaths are preventable, if given the appropriate tools for accurate diagnosis. Due to lack of suitable diagnostic tools, clinical treatment in low resource settings is initiated based on patient symptoms and regional prevalence. A practice referred to as syndrome-based management. Syndrome-based management can be effective for treating diseases with clear and distinct symptoms. Pneumonia, influenza, dengue, and many other infections present

with similar symptoms, such as fever. As a result, using only syndrome-based management, a child presenting with early onset fever in malaria-endemic regions may be automatically treated with anti-malarial drugs. This child could have a fever from another infection that left untreated could result in disability or death. The misuse of anti-malarial drugs is one of the culprits behind the increase in anti-malarial drug resistance [6]. Accurate diagnosis has the potential to both improve patient outcomes and reduce the global disease burden.

Point-of-care (POC) diagnostics is a class of diagnostics that is increasingly being recognized for its ability to provide rapid results for earlier treatment, resulting in improved clinical outcomes [7]. Current POC diagnostic methods, such as lateral flow tests (LFTs), targeting many infectious disease targets in the developing world are inexpensive and easy to use, but lack clinical sensitivity. In contrast, current laboratory-based diagnostic tests, such as ELISAs (enzyme linked immunosorbent assays), have the necessary sensitivity but are not applicable to patients in developing world settings due to high cost, temperature dependent components, long time to results, and the requirement of trained personnel to perform or maintain instrumentation integral to the test. Thus, there is a medical need for improved POC diagnostic tests that combine the advantages of LFTs with the enhanced sensitivity and sample processing capabilities of laboratory-based tests.

Recently, the Fu/Lutz/Yager group has introduced paper-based devices called two-dimensional paper networks (2DPNs) that enable the performance of both simple and complex multi-step assays. 2DPNs have the potential to carry out the sophisticated capabilities of high sensitivity laboratory-based tests using the same principles and inexpensive materials of LFTs while keeping user activities to a minimum. The ability of 2DPNs to deliver multiple reagents in a

step-wise manner through a common detection region allows for the implementation of additional reagent delivery formats for carrying out an immunoassay. The effect on the signal and time to result for these alternate reagent delivery formats has yet to be characterized in a paper-based system. Conventional LFTs use a dry premix format for a rapid one step delivery of two detection reagents: analyte and colorimetric label. With 2DPNs, the sequential delivery of analyte and colorimetric label, as well as the addition of rinse and amplification steps, is possible. 2DPNs have the potential to achieve higher sensitivity by enabling changes in the method reagents are delivered compared to LFTs.

1.2 Proposed Solution

This project seeks to investigate and design more sophisticated 2DPN assays using the malaria antigen *Plasmodium falciparum* histidine-rich protein 2 (PfHRP2) as a model analyte. This project first uses three different paper fluidic tools to create amplified assays that include a rinse to minimize nonspecific absorption and delivery of reagents for signal amplification. This project then investigates the delivery format-dependent signal generation and binding pattern and its implication for higher-sensitivity detection in 2PDNs. Conventional LFTs use a rapid one step delivery of analyte and colorimetric label (premix delivery). 2DPNs allow the step wise delivery of analyte and colorimetric label (sequential delivery) using the same reagent system. Protocols for carrying out the two delivery formats, premix and sequential, are developed. The assays are characterized and the results are compared to understand the differences in the spatial distribution of the binding patterns and signal intensity changes with the different formats.

1.3 Layout of Thesis

This chapter lays out the problem with current POC diagnostics in low resource settings and provides a proposed solution in the form of utilizing alternate delivery formats in 2PDNs. Chapter 2 provides key background information on POC diagnostics, basic principles of flow in porous media, and a literature review of the state of the art. Chapter 3 presents detailed information on the malaria protein model system and highlights different methods for fluid control worked on by the author, in collaboration with Barry Lutz, Jared Houghtaling, Bhushan Toley, and Brittney McKenzie, and translated into 2DPNs.

Chapter 4 experimentally investigates the format-dependent spatial distribution of the signal intensity. Chapter 5 details the development of experimental protocols for the premix and sequential delivery of reagents in the context of PfHRP2 protein detection. The limit of detection (LOD), a measure of sensitivity is determined for both premix and sequential deliver formats in Chapter 6. Additional background, methods, results, and conclusions will be elaborated on within the chapters.

Chapter 7 discusses the overall conclusion and implications of this work. Suggestions for future work will be presented.

Chapter 2: Point-of-care Diagnostics

2.1 Point-of-care (POC) Design Requirements

Infectious diseases have their highest burden in the developing world [8]. In the developing world, laboratory facilities can be limited by poor or unreliable supplies of fresh water, electrical power, and few/and or untrained personnel. For any POC test to have functional value, it must stand up to the constraints presented by the present healthcare infrastructure in developing countries. The World Health Organization (WHO) Sexually Transmitted Disease Diagnostics Initiative developed the well-accepted ASSURED criteria as general guidelines for the development of a POC diagnostic test. The guidelines states that diagnostics should be: Affordable, Sensitive, Specific, User-friendly, Rapid and robust, Equipment-free, and Deliverable [9].

In most malaria-affected countries the annual expenditure per capita on all aspects of health is less than $ 10 [6]. Patients typically pay out of pocket for services that exceed the cost of treatment [6]. To have clinical utility, any diagnostic test must be reliable and accurate. Sensitivity and specificity are important measures of test accuracy. The WHO has recommended a minimal standard of 95 % sensitivity for P. falciparum densities of 100/µl and a specificity of 95 %. In remote settings, patients often travel extensive distances for medical attention, rapid diagnosis allows for treatment during the initial and often only visit to the local clinic. A practical test should maintain function in areas with harsh environmental conditions, poor delivery infrastructure, and absence of reliable electricity.

The traditional method of high-magnification transmission light microscopy, where a stained blood smear sample is used to identify malaria parasite levels, is still the gold standard for

malaria diagnosis. While sensitive, the cost of the equipment and trained personnel necessary to perform such a method limits its applicability in malaria endemic regions. In the recent years, several commercial LFTs for malaria are being implemented. However, their performance is highly variable [10, 11] . The increase in drug resistance has made specific diagnosis of malaria both more cost effective and elevated the need for a more accurate diagnostic module. In previous decades, chloroquine - widely available, safe, inexpensive, and effective – was routinely used for patient presenting with symptoms of malaria infection. The emergence of chloroquine resistant malaria and the introduction of expensive artemisinin combination therapies as the first-line treatment has changed the cost-benefit ratio of treating all patients presenting with fever with malaria drugs [6, 12].

Conventional microfluidic and paper-based technologies have been investigated as alternative methods for diagnosis in low resource settings to address the challenges presented by the ASSURED criteria. The main advantage of these technologies is the potential capability for miniaturization and automation of complex laboratory processes.

2.2 Microfluidics

Microfluidic devices are becoming attractive for point-of-care diagnostic applications. Microfluidic devices are comprised of networks of ducts patterned into silicon, PDMS, or plastics. Their small size and sample volumes reduce the overall test cost, and length of assay time without compromising sensitivity and specificity [7, 13]. Driven by pneumatic or pressure pumps, fluid flow can be easily manipulated making multistep chemical processes both possible and controllable.

Commercially available microfluidic-based POC systems exist, such as blood glucose monitors, but have mainly been limited to developed countries. The Yager lab at the University of Washington and its collaborators have developed an automated microfluidic diagnostic system known as the DxBox for the detection and analysis of multiple fever causing agents prevalent in the developing world. However, the complexity, cost, and maintenance requirements limit its adoption in remote clinical environments.

Paper-based diagnostics offers a potential avenue to mitigate the complexity, cost, and maintenance requirements characteristic of many conventional microfluidic systems. The principles behind paper-based diagnostics and discussion of the most common paper-based diagnostic test, the lateral flow test (LFT), is discussed in the following sections.

2.3 Paper-based Fluidics

Paper-based microfluidic technologies hold great potential to deliver POC diagnostics to the developing countries and meeting the ASSURED criteria. As a class, paper-based diagnostics utilize microporous paper materials as substrates for carrying out assays. Porous materials enable the use of capillary action for fluid control eliminating the necessity for external pumps. The materials themselves are inexpensive, easy to manufacture, and easy to manipulate.

2.3.1 Lateral Flow Tests

LFTs are disposable, rapid, user-friendly, and inexpensive. The user simply adds sample to the test, and fluid transport occurs due to capillary pressure of the porous paper material, eliminating the need for pumps. The sample mixes with a detection label (e.g. antibody conjugated to a label) stored dry in a conjugate pad. The analyte-label complex continues to flow through the porous

membrane until it is captured at a test line via an immobilized capture molecule (e.g. antibody) (Figure 2).

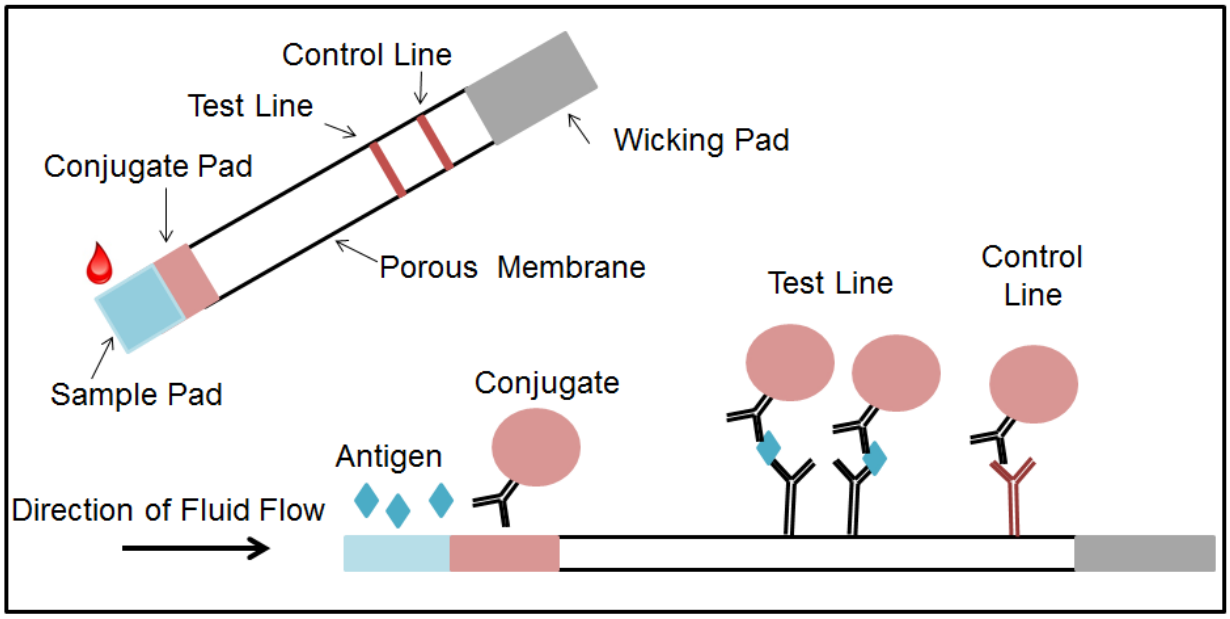

Figure 2. Schematic of a Lateral Flow Test. Sample is added to the sample pad. Upon flow through the conjugate pad, the sample rehydrates conjugate and continues to flow through the porous membrane. Signal is generated at the test and control lines in the event that antigen-conjugate is captured at the test line and conjugate is captured at the control line. The wicking pad continues to drive flow after the wet-out of the porous membrane.

The analyte-label binding event to the immobilized capture molecule produces qualitative yes or no signal. In the absence of analyte, no binding event will occur at the test line and no signal will be visible. The simplicity, speed, and cost make LFTs useful for diagnosis of analyte where the clinically relevant concentration of analyte is high in solution. For diseases where the clinically relevant concentration of analyte is low, LFTs are not suitable for higher sensitivity detection. LFTs are limited to performing simple one step chemical processes; therefore, they cannot achieve the same sensitivity that multistep laboratory-based tests, such as ELISA, can produce.

Thus, LFTs lack clinical utility for disease targets requiring a high analytical sensitivity, such as malaria.

2.4 Basic Flow Principles

Nitrocellulose "paper" is the most common porous substrate utilized in LFTs. Nitrocellulose membranes with high homogeneity and specific capillary flow properties are available from several companies and are well-characterized, convenient materials for paper-based tests. Understanding fluid flow in porous media like nitrocellulose is of upmost importance for the design of paper-based tests.

A porous material can be defined by many characteristics. The nitrocellulose membranes used for this work has a pore size between 8 to 15 µm. Because the pore size in widely variable within the membrane, the pore size distribution gives a more accurate representation of the porous material. The increase in capillary flow rate –speed a fluid front travels through a membrane- is associated with a shift in pore size distribution toward higher pore sizes. The fluid capacity and fluid flow is affected by the void space in a material. The membrane porosity is a measure of the total volume of liquid needed to wet out the membrane. Porosity and capillary flow rate exhibit a positive linear relationship.

In order to understand the flow of fluid through our porous media, approximations need to be made. The variable nature of the membrane morphology makes modeling the fluid flow behavior complex. A common approximation is to treat the membrane as an array of cylindrical pores. The porous membrane exhibits laminar flow behavior, where mixing is dependent on diffusion alone. Laminar flow is defined by a low Reynold's number (<2100), a ratio of inertial forces to

viscous forces. The paper devices to be discussed exhibit laminar flow. Membrane pore diameters are typically between 1-10 μm resulting in Reynold's numbers on the order of 10^{-3} at the typical velocity flow rates for lateral flow membranes of around 10^{-1} m/s.

Fluid flow is driven by a difference in pressure known as capillary pressure, which is given by:

$$\Delta P_{capillary} = \frac{2\gamma \cos\theta}{r}$$

where r is pore radius, θ is the fluid wetting angle, and γ is the surface tension at the air-water interface. Wet out of a porous membrane can be described by the Washburn equation [14]:

$$L^2 = \frac{\gamma d t}{4\mu}$$

where d is the pore diameter, t is the time it takes a fluid front to initially wet out a porous material of length, L, μ is the fluid viscosity, and γ is the surface tension of the fluid. Based on the equation, the distance travelled by the fluid front is related to the square root of time and a function of pore diameter, fluid viscosity, contact angle, and fluid surface tension.

Fluid flow in a fully wet out membrane exhibits Darcy's flow [15] which follows:

$$Q = -\frac{\Delta P}{\frac{\mu l}{kA}}$$

where Q is volumetric flow rate. The denominator term represents the resistance which is inversely related to the permeability of paper (k) and area (A), and directly related to the viscosity (μ) and length (l).

2.5 Immunoassays

Immunoassays employ the use of an antibody to measure the presence or concentration of an analyte (antigen) of interest from a sample, often a biological liquid such as serum or urine. Antibodies are specific proteins secreted and used by the immune system to recognize specific antigen. Typical antibodies have two distinct regions: a variable (Fab fragment) region and a relatively conserved (Fc fragment) region. The portions of the antibody and antigen responsible for binding are referred to as the paratope on the antibody and the epitope on the antigen. A total of five classes of antibodies exist. IgM and IgG are the most commonly used in immunoassays. An IgG, smaller around 150 kDa, has two paratopes while an IgM, larger around 970 kDa, has 10 paratopes [16]. These differences in size and number of binding sites play a considerable role in selection and performance of antibodies used in immunoassays.

Immunoassays often require multiple timed steps, but some immunoassays, like that carried out in LFTs, requires simple mixing of reagents and sample. The basic principle behind an immunoassay is the binding of an immobilized antibody to a specific analyte in a heterogeneous sample to produce a measurable signal. The affinity, or how tightly the antibody binds to the analyte, can be described the dissociation constant, K_d, represented by the following equation:

$$K_d = \frac{[Ag][Ab]}{[AgAb]}$$

where [Ab] is the molar concentration of antibody, [Ag] is the molar concentration of antigen, and [AgAb] is the molar concentration of antibody-antigen complex at equilibrium.

2.5.1 Types of Immunoassays

Immunoassays can be classified into three categories: direct, indirect, and competition. This body of work will focus on direct immunoassays (Figure 3).

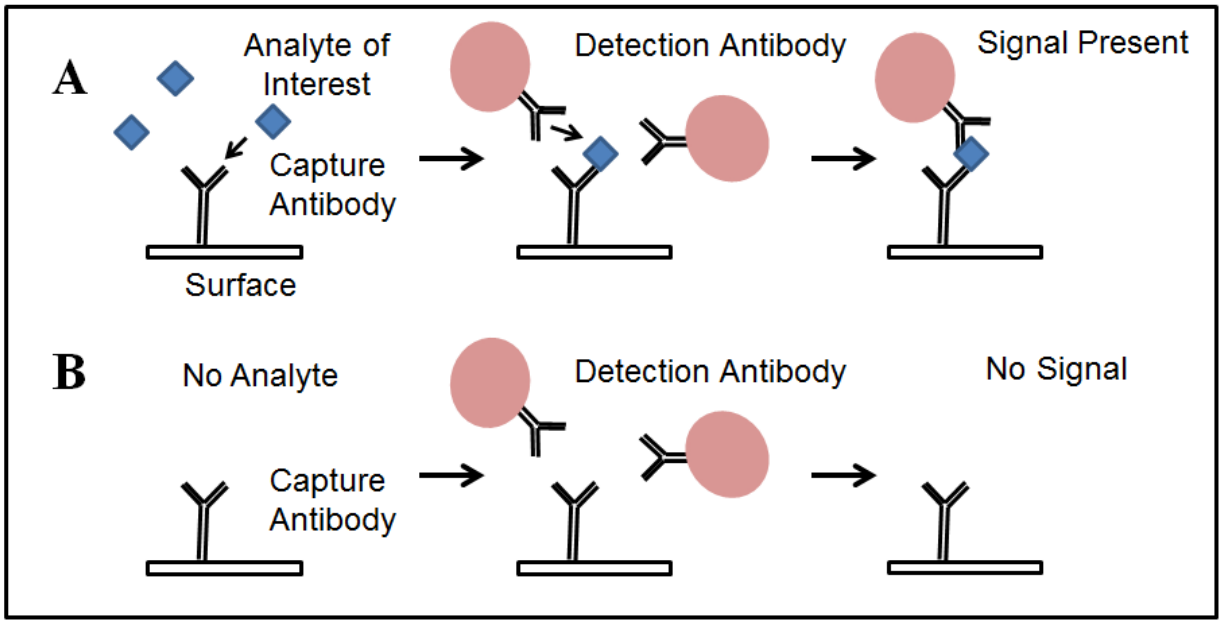

Figure 3. Direct Immunoassay Schematic. (A) In the presence of an analyte, a signal is produced. An antibody specific to the analyte of interest is immobilized to a surface and acts as a capture molecule. Analyte is introduced and is captured by the capture molecule. Introduction of detection molecule (antibody conjugated to a label in this case) binds to the analyte of interest and a signal is produced. (B) In the absence of an analyte, no signal is produced.

In a direct immunoassay, an antibody specific to the target of interest acts as a capture molecule that binds to any target of interest that is introduced via the sample. A detection molecule, typically an antibody conjugated to a label, is introduced and binds to the antigen of interest creating a "sandwich". The assay signal is a measurement of signal produced by the sandwich formation.

Signal measurement depends on the label conjugated to the detection antibody. Colorimetric labels are especially convenient for untrained users for qualitative yes/no answers. Colorimetric labels, such as carbon beads or gold nanoparticles, are the most commonly used in LFTs [17]. Several higher sensitivity colorimetric labels are widely employed especially in lab-based settings including fluorescent dyes or enzyme-based labels. Fluorescent dyes, unlike colorimetric

beads and nanoparticles, require an external reader. Enzyme-based labels often require an extra set of reagents compared to colorimetric beads and nanoparticles. A very common enzymatic system, ELISA has been implemented in LFTs for its amplification and quantitative properties [18-21]. Table 1 compares the enzymatic, fluorescence, and colorimetric bead/nanoparticle systems.

Table 1. Comparison of the common detection mechanisms.

Detection Mechanism	**Advantages**	**Disadvantages**
Enzymatic System	Single enzyme can catalyze many reactions yielding high sensitivity	Typically requires many more reagents compared to other detection mechanisms
Fluorescence	Potential to be very sensitive due to low background signal	Requires an external detector
Colorimetric Bead or Nanoparticle	Easily visible by the naked eye	Sensitivity is often an issue

When gold nanoparticles are used alone, a pinkish colored visible signal is produced when the binding event occurs. For high concentrations of analyte, the visible signal will be pronounced. At low concentrations of analyte though, the signal may be faint or not visible. The signal can be enhanced via signal amplification. Amplification results in an increase in the visible signal at all concentrations of analyte including the previously faint/not visible signals. Conventional LFTs cannot perform the signal amplification step described above because they are limited to one step chemical processes. 2DPNs can implement the multiple reagent deliveries necessary for signal amplification chemistries.

2.6 Current State of Art

In 2008, the Whitesides group demonstrated the use of patterned cellulose carrying out one-step chemical processes to detect both glucose and protein in urine samples [22]. Since then, interest in the use of porous materials in POC devices has grown. Martinez et al. described "a new class of analytical devices fabricated by layering paper patterned into hydrophilic channels and hydrophobic walls and tape patterned with holes that connect channels in different layers of paper". These 3D paper networks, or so-called 3D μPads, extend beyond simple lateral flow of fluid to both lateral and vertical flow of fluid through paper [22, 23]. The manipulation of the hydrophobic and hydrophilic properties of materials to outline a path for fluid flow in paper is now conventional practice for fabrication of a majority of paper-based devices. Schilling et al. recently presented a new method for μPads fabrication that utilizes toner as the "glue" to bind multiple layers of paper together [24, 25]. Wax printing to create hydrophobic wax walls has been an alternative method for outlining channels for fluid flow through paper [26]. Abbas et al. demonstrate a simple cut and drop method for the creation of their paper-based analytical μPad using the natural capillary effect of paper to concentrate reagents into localized regions and enable subattomolar detection [27]. Many new methods in the area of paper-based fluidics have been made in terms of device fabrication. Nie et al. describe a new one-step fabrication method for paper-based devices. They used commercially available permanent markers and metal templates which have been etched with specific patterns to plot pattern onto paper. Ink acts as the hydrophobic barriers to flow. The process according to Nie et al. takes under a minute and does not require specialized equipment or skills [28].

Other groups have demonstrated paper-based tools to control fluid flow in paper. Zhao et al. used chlorinated polyvinyl chloride to create a barrier to fluid flow in filter paper in a new microfluidic paper-based device to detect nitrite contamination in water, which is another

application of simple paper-based devices outside of direct detection of infectious diseases [29]. Zhou et al. propose the use of threads as a support for transporting and mixing liquids in paper-based assays [30]. However, they failed to demonstrate high sensitivity, thus there is still potential for the use of threads as a tool for transportation but there are obvious barriers to overcome. Several groups have made developments in microfluidic valves (i.e. on and off switches) for paper systems for fluid control. Backer et al. developed two types of microvalves that are temperature responsive and pH responsive. Hydrogel films are prepared directly inside a channel and the swelling and shrinking properties of the films act to connect and disconnect fluid flow through the channels [31]. Chen et al. created a fluidic diode fabricated entirely out of a single layer of paper to control fluid wicking. The fluidic diode can be used to stop fluid and also as to delay fluid through paper and manipulate fluid flow timing [32]. Work by the author on fluid control tools in the context of paper-based diagnostics will be presented and discussed in Chapter 3.

Recently, several groups have published paper-based platforms for carrying out multi-step assays to include sample pretreatment and purification. Yang et al. developed a µPad utilizing paper fibers for blood purification and subsequent one step colorimetric detection [33]. Apilux et al. demonstrated a paper-based device for carrying out a sandwich ELISA requiring only the user introduction of a sample solution by creating delay zones within the paper membrane [34]. The delay zones were created using a special ink jet printing technique to create baffles to achieve fluid delay. Gerbers et al. report a device made of paper and tape incorporating valves developed by Chen et al.[32]. The valves are embedded within the membrane layers and enable the sequential delivery of three fluids [35]. A linear paper network referred to as a Pseudo-1DPN was introduced to perform clean sequential fluid delivery using wells as fluid sources while

reducing device running time [36]. While the linear paper network design is simple, it was found that glass fiber source pads required an increase in the length between the fluid sources. The result is an increase in the footprint and the running time of the device.

Recent work by the Fu, Lutz, and Yager groups have focused on the development of a two dimensional paper network (2DPN) technology that is based on the strengths of LFTs, but allows for complex chemical processing. More background on 2PDN development will be presented in Chapter 3. Briefly, 2PDNs make use of multiple inlets to which different reagents may be introduced. The multiple inlets eventually feed into a common detection channel (Figure 4). With multiple inlets per detection region, sequential application of multiple reagents to the detection region can be implemented to perform automated multistep processes.

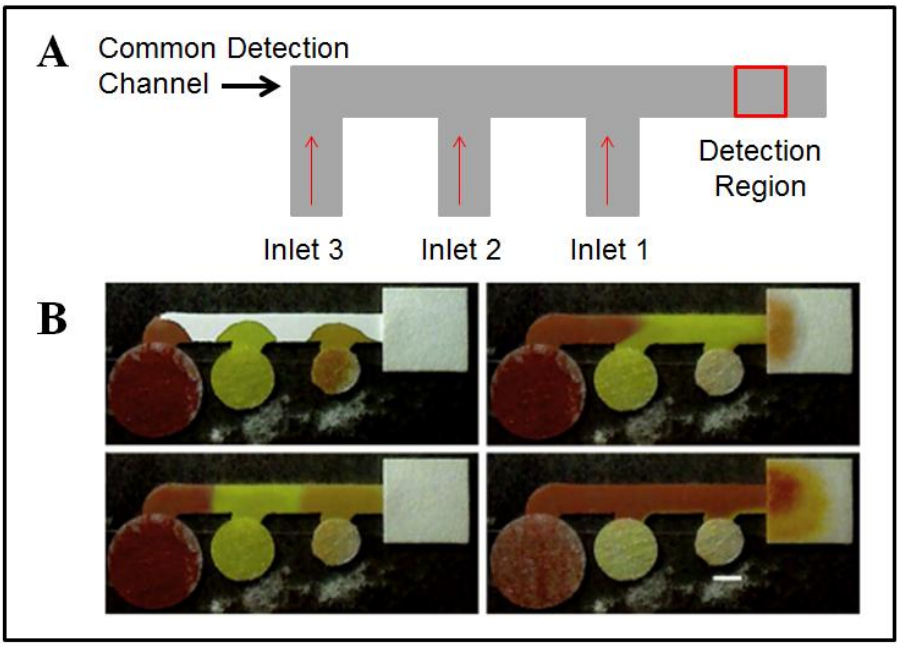

Figure 4. Sequential delivery in a 2PDN enabling multistep chemical processing. (A) Schematic of 2DPN with multiple inlets per detection region enables automated multistep processes. (B) Image series of timed sequential

delivery of three different fluids from three separate inlets. 2DPNs offer improved control of fluid delivery compared to conventional LFTs. Figure adapted from Fu et al. [37].

2.7 Conclusions

Conventional microfluidic and paper-based microfluidic devices are becoming attractive for point-of-care diagnostic applications. Driven by pressure pumps, fluid flow in microfluidic devices is easily controllable. These pneumatic pumps often require external instrumentation. Paper-based devices take advantage of the capillary driven flow characteristic of paper to drive fluid flow. The absence of required external instrumentation, low cost of materials, and minimum user training required make 2DPNs more usable for low-resource settings than conventional microfluidic-based devices. With 2DPN development and paper-based diagnostics as a class there is a need for an improved understanding of the advantages and disadvantages of translating multi-step assay protocols into paper. 2DPNs offer the potential to improve the sensitivity of LFTs by integrating multiple assay steps. The particular focus of this project is to contribute to high-sensitivity assay development, through the automation of multistep processes for signal amplification and the investigation of the effect of different reagent delivery formats on the generated signal intensity and limit of detection of the assay.

Chapter 3: Two-dimensional Paper Networks in the Context of Malaria Detection

3.1 Two-dimensional Paper Networks

Two-dimensional paper networks (2DPNs) are a class of paper-based devices, in which instead of the one dimensional linear strip format of LFTs, porous media is cut into various geometries based on utility [38]. Nitrocellulose is typically cut into a design where multiple channels eventually feed into a common detection channel (Figure 4). The multiple channels per detection region allow for the input of different reagents and with the appropriate fluid control tools enable the step-wise timed delivery of the reagents. The following sections will first describe the malaria model system and proceed to highlight work done demonstrating automated signal amplification in three different 2PDN devices.

3.2 Malaria Model System

Malaria ranks 7th in global disease burden according to the new Global Burden of Disease Study published in 2012 [39]. The tests most widely used for diagnosis of malaria infection target the parasite antigen histidine-rich protein 2 (HRP2). Current malaria LFTs are insufficient for accurate diagnosis [40, 41]. This makes a *Plasmodium falciparum* Histidine-rich protein 2 (PfHRP2) a medically relevant model. As a benchmark for any sensitivity measurements discussed later, Table 2 outlines published limits of detection for a variety of malaria diagnostics.

Table 2: Reported limits of detection for a variety of malaria diagnostics[a].

Method	Reported Limit of detection [ng/ml]
ELISA	0.1-4 ng/ml [18, 42, 43]

In-lab LFTs[b]	6.94-27.75 ng/ml [44]
LFTs in the field	Varies widely ~ 90 ng/ml [10, 11]

[a] Table based on table created by Gina Fridley [45]
[b] FirstSign™ ParaView, SD BIOLINE Carestart™, ICT Malaria Combo Cassette

2PDNs have the potential for improved sensitivity compared to LFTs. The automated multi-step processing capability of 2DPNs can implement multi-step chemical processes, such as ELISA, and retain the user-friendliness and reduced time to result of LFTs.

3.2.1 Immunoassay Stack

A murine PfHRP2 antibody (Immunology Consultants Laboratory, Portland, OR) acts as the capture molecule and is patterned to form a test line with a piezoelectric inkjet printer onto nitrocellulose membranes. The specific PfHRP2 antibody shows the best potential for use in a LFT according to data presented by Lee et al. in a study comparing the prevalence and frequency of epitopes and heat durability profile of eight commonly used PfHRP2 monoclonal antibodies [41]. An anti-mouse antibody is patterned to serve as a control line downstream of the test line. A recombinant PfHRP2 (CTK Biotech, San Diego, CA) serves as the analyte of interest with 18 epitopes and is delivered spiked into fetal bovine serum (Invitrogen, Carlsbad, CA). A second PfHRP2 murine antibody (Immunology Consultants Laboratory, Portland, OR) is custom conjugated to a gold nanoparticle (BBInternational, Cardiff, UK). Each gold nanoparticle is conjugated to an average of twelve antibodies for a total of twenty four possible binding sites. A commercially available gold enhancement (GE) solution (Nanoprobes, Yaphank, NY) was used as the signal amplification reagent for this body of work. Figure 5 is a schematic of the complete malarial assay stack including the amplification step.

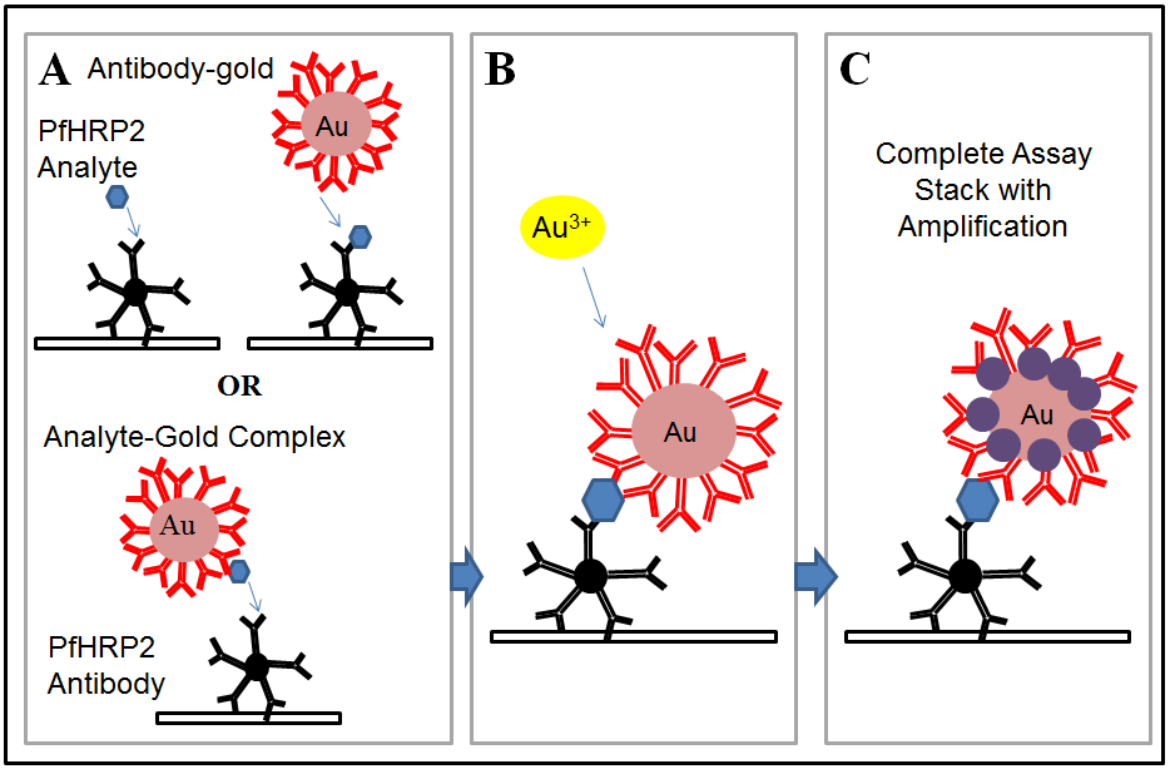

Figure 5. Schematic of malaria assay stack. (A) In sequential format, PfHRP2 analyte binds to immobilized PfHRP2 IgM followed by antibody-gold binding to the analyte (top). In premix format, an analyte-antibody-gold complex binds to the immobilized PfHRP2 IgM (bottom). (B) Gold enhancement solution reacts with the gold nanoparticle in the IgM-analyte-antibody-gold. (C) Complete assay stack with amplification results in a dark purple signal.

The particular signal enhancement chemistry illustrated here and used in this body of work is a metal catalytic reaction. A solution containing a gold salt is mixed with a reducing agent causing the gold salt to reduce to gold atoms on the surface of the nanoparticle. The gold ions from the salt are reduced and deposited onto the surface of the nanoparticle [46-48]. The nanoparticle size increases and its light absorption spectrum changes. The subsequent increase in size of the nanoparticle/gold deposits causes the signal color to change from pink to dark purple [37, 49, 50]

3.3 Overview of Device Materials and Fabrication Techniques

Several different fabrication techniques for paper-based devices were described in Chapter 2.6. The methods previously described have demonstrated utility for fabrication of paper-based devices; however, a disadvantage of many of the methods is the complexity of the fabrication process and the resolution. Our lab uses a commercial CO_2 laser system for the fabrication of not only nitrocellulose paper network but also both porous, such as glass fiber for sample and reagent pads, and nonporous device components, such as Mylar for the device housing. With our CO_2 laser system, we can create paper networks with complex features at high resolution in a one-step process. By varying the cutting parameters for the same material, a material can be cut through to create a distinct fluid path or etched to help align device components during the fabrication process. Figure 5 (top) shows an example of a paper network assay made using the CO2 laser system. The Mylar/adhesive substrates were cut using a higher power to cut through the plastic and a lower power to simply etch the surface to help align the cellulose, nitrocellulose, and glass fiber components. Typical laser power, translation speed, and number of passes for device fabrication for the materials shown in the paper network assay are provided in Figure 5 (bottom).

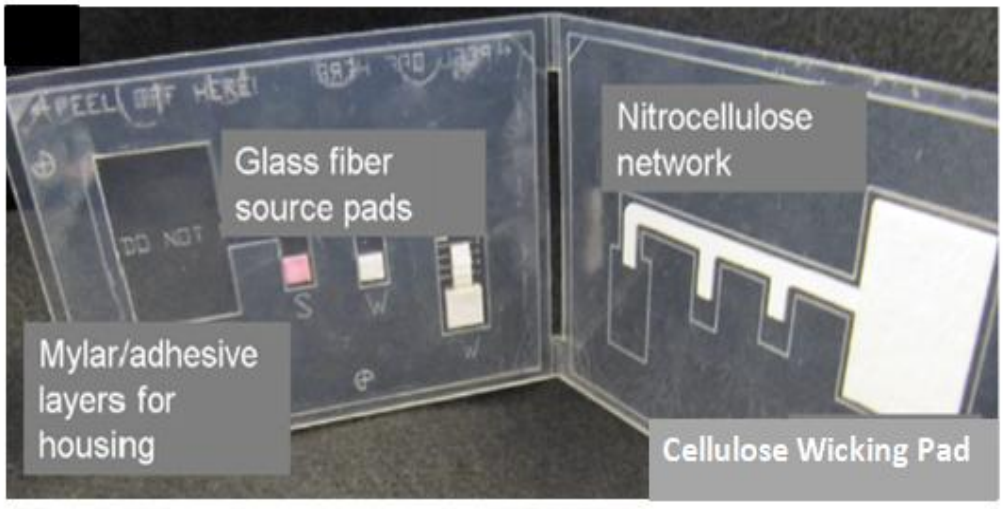

Material	Power (W)	Translation Speed (mm/s)	# of Passes
Nitrocellulose	2	8	1
Glass Fiber	1	3	1
Cellulose	4	14	2
Mylar (10 mil) with adhesive on one side (through)	16	12	1
Mylar (10 mil) with adhesive on one side (etched)	3	12	1
Mylar (20 mil) with adhesive on both sides	23	12	1

Figure 6. Paper-based device components are cut using a CO2 laser system. Prototype paper network device [50] fabricated with components cut with the CO2 laser system (top). Typical laser system settings for cutting various materials used in our paper network devices. Table adapted from a table presented in a technical note [51] bottom.

3.4 A 2DPN using Paper Geometry to Enable a Multi-step Assay

The power of the 2DPN lies in its ability to carry out timed, multi-step chemical processes. In a 2DPN that relies only on the membrane for fluid control, manipulation of paper geometry provides a method for achieving sequential delivery of multiple reagents. The time a particular reagent reaches a detection region is dependent on the path length between the inlet and the detection region. The differences in capillary pressure between the source materials, membrane, and sink material affect both the amount of fluid volume released and the volume release profile.

Figure 7 shows programmed sequential delivery in a 3-inlet 2DPN. Contact is between glass fiber source pads of varying sizes and the membrane activates fluid flow in all three inlets

simultaneously. The fluids arrive in the order of yellow, red, and blue with limited co-flow of multiple colors over the detection region.

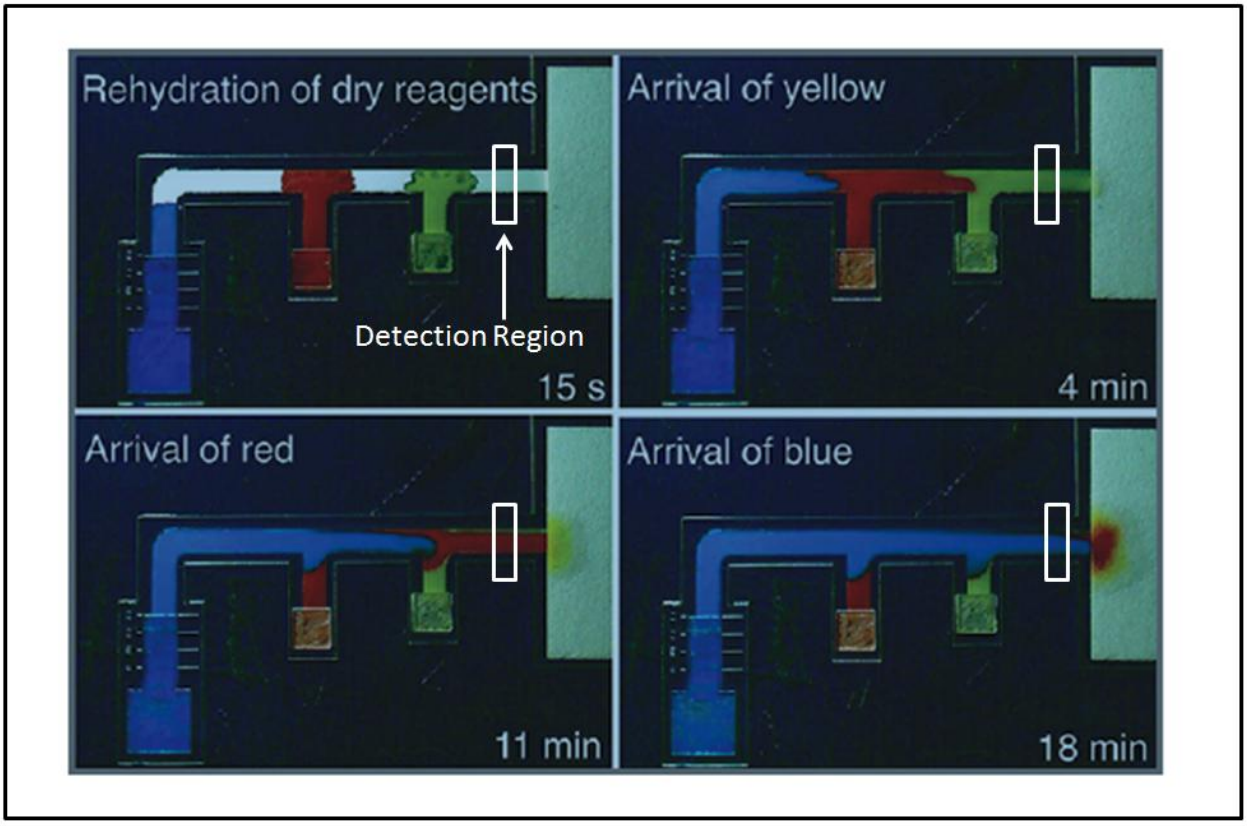

Figure 7. Visualization of the sequential delivery of three fluids in a 2DPN. Image series shows the sequential delivery of three fluids (10 µl yellow, 10 µl red, and 40 µl blue) through the detection region labeled. Activation of fluid flow into the inlets resulted in the staged delivery of yellow, red, and then blue through the horizontal leg. Image from Fu et al [50].

A 2DPN was designed to carry out three chemical steps: 1) delivery of analyte and gold conjugate, 2) a rinse step after the gold conjugate premixed with analyte has bound to the capture antibody, and 3) a signal amplification step. The main components of the card are labeled (Figure 8).

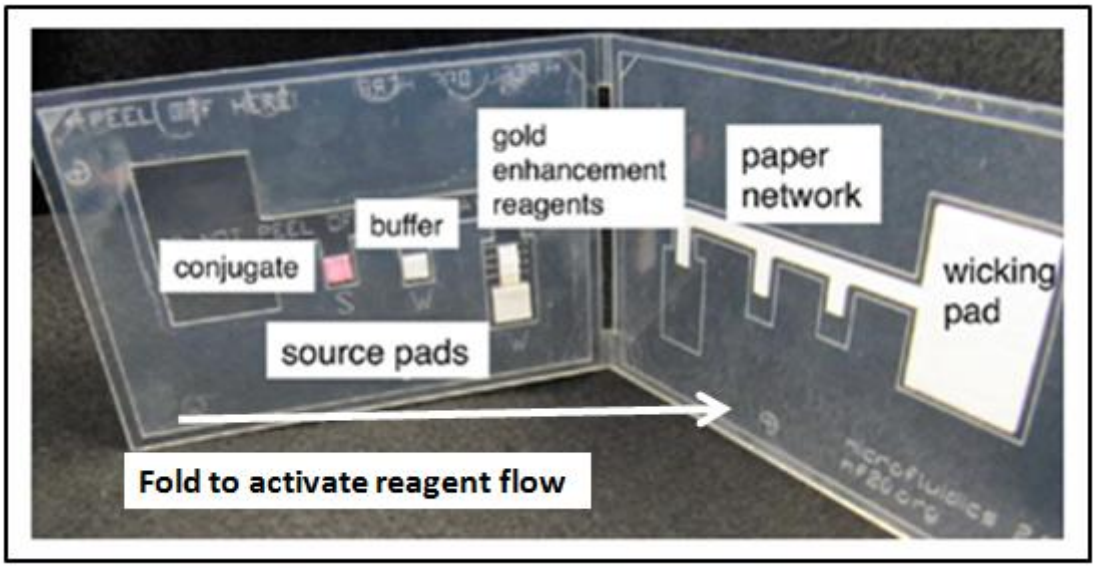

Figure 8. 2DPN card format demonstrated for an amplified immunoassay. Conjugate, buffer, and gold enhancement reagents are stored dry on the left side of the card. The addition of fluid rehydrates the reagents at the time of use. The user adds sample to the pad labeled "S" and water to the pads labeled with "W" and folds the card to activate reagent delivery to the paper network. A wicking pad drives fluid flow through the paper network. Figure adapted from Fu et al [50].

The user simply adds sample and water to the appropriate locations on the left side of the card (Figure 8) and folds the card in a single activation step. The flow of the reagents is shown using colored fluid in Figure 7: yellow (sample), red (rinse), and blue (signal amplification reagent). The sample rehydrates the gold conjugate solution that is stored dry in a glass fiber pad. Once the sample plus gold conjugate reaches the detection region, in the presence of the analyte, a signal comparable to the signal from a conventional LFT is produced (Figure 9 top). The arrival of the rinse removes any nonspecific adsorption. Finally, once the signal amplification reagent reaches the detection region, the original signal is amplified (Figure 9 bottom).

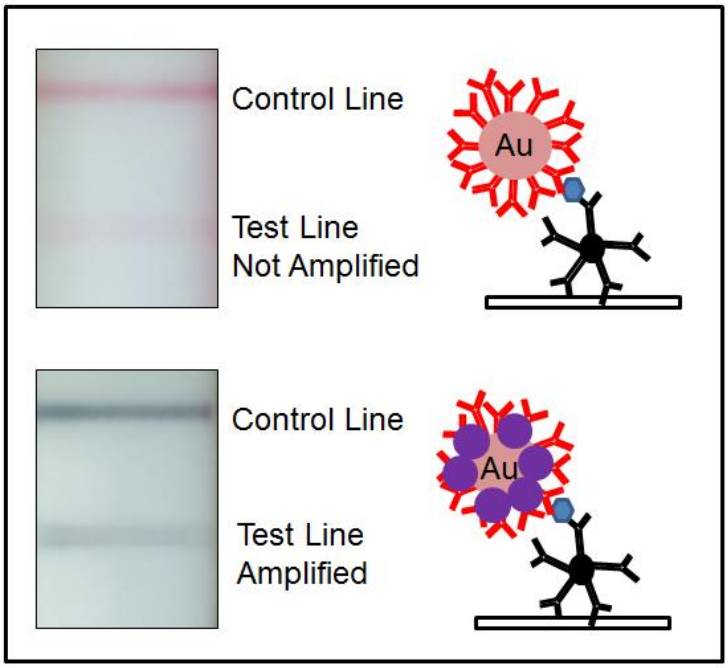

Figure 9. Schematic of Assay stack and corresponding signal at each step. Signal generated from the binding of analyte bound to gold conjugate to the capture antibody at a PfHRP2 concentration of 20 ng/ml (top) and amplified signal at 20 ng/ml (bottom).

The geometry of the paper network is critical to the sequential delivery of the three fluids. The distance between each inlet and from the detection region is such that there is limited co-flow of two fluids through the detection region. The 2DPN described in this section has two important features besides the geometry of the network: volume metering and dry reagent storage. Volume metering is achieved by using source pads of varying fluid capacities. All reagents in the assay minus the sample were stored in dry form on the card. The gold enhancement reagent used requires combining four separate reagents immediately prior to use. Once combined over extended periods of time (~ 30 minutes), the solution auto nucleates and produces a high nonspecific background, thus greatly reducing the assay sensitivity. The four reagents are dried separately in source pads. The reagents were rehydrated with water after 1 week and 4 weeks of dry storage and the signal from the rehydrated solutions were compared to fresh reagent. The

signals from rehydrated and fresh GE solutions were within 15 % of one another. The small loss of signal between fresh and rehydrated suggests that the GE solution retains its amplification properties even after at least up to 4 weeks of dry storage.

The signal response curves for the amplified assay and the unamplified assay are shown in Figure 10.

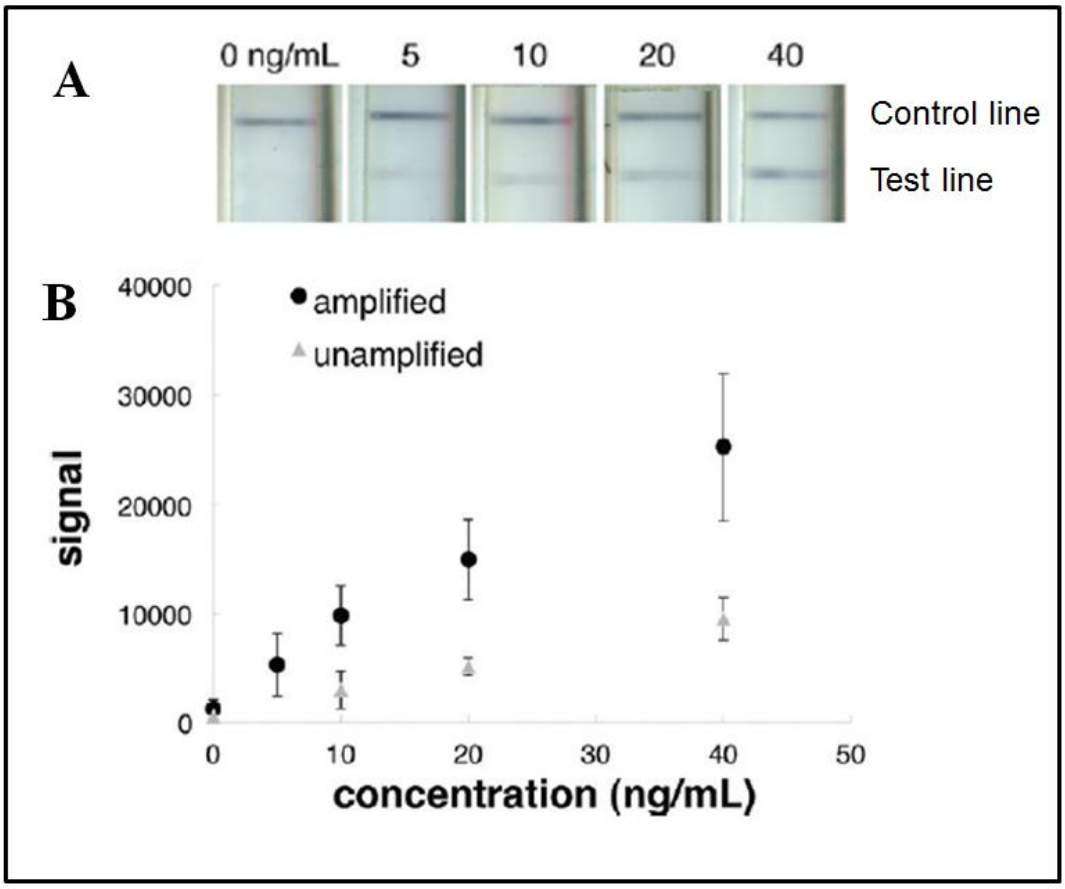

Figure 10. 2PDN assay results. (A) Image series of the detection region at different concentrations of PfHRP2 analyte after amplification. (B) Signal response curves for the amplified assay and unamplified assay represent average signal for each concentration. For the unamplified case, additional water rather than old enhancement reagent was run in the 2PDN card format. Data points represent the average of 4 measurements. The data point for 20 ng/ml is the average of 3 measurements. Error bars represent the standard deviation. Image adapted from Fu E, Liang, T et al. [50].

An unamplified assay refers to a 2DPN run with no signal amplification reagent instead an extra volume of rinse buffer is delivered. A total of 36 tests (4 tests at each at 40, 20, 10, 5, and 0 ng/ml for the amplified case and 40, 20, 10, and 0 ng/ml for the unamplified case) were run and analyzed to produce the signal response curves. The detection region of each card was scanned and then processed using a custom analysis program (Matlab, Natick, MA). Analysis details are elaborated in Chapter 4. The signal is defined as the average grayscale intensity at the test line subtracted from the average grayscale intensity in a background region upstream of the test line. The limit of detection of the amplified 2DPN malaria card was 2.9 ± 1.2$\frac{ng}{ml}$. The limit of detection of the unamplified 2DPN card was 10.4 ± 4.4$\frac{ng}{ml}$. The amplified 2DPN produced an approximately fourfold gain in sensitivity over the unamplified case. Though, this sensitivity gain is modest, we demonstrated the sequential delivery of multiple reagents for carrying out a multistep signal amplified assay in a 2PDN format. Different signal amplification chemistries may be able to achieve higher sensitivity gains in a 2PDN format. Preliminary work and current state of the art suggests even greater gains in sensitivity are plausible [17, 21, 46].

Design of the paper geometry is a simple and inexpensive method for controlling the timing of fluid flow through a detection region. Fluid flow can be controlled without the use of another material which eliminates potential errors due to material to material contact. The major drawback though of simple geometry for controlling fluid flow is the size the device must be to carry out assays requiring high(er) volumes or more steps. The timing of fluid flow is dependent on the path length between the fluid inlet and the detection region. Thus, more steps require more extensions and higher volumes require even longer path lengths to prevent temporal delivery of

multiple reagents. Extensions also means the fluid requires extended time to reach the detection region and can extend the assay time greatly.

3.5 2DPNs using Alternative Methods to Enable a Multi-step Assay

Flow in 2DPNs can also be controlled using techniques such as dissolvable sugar barriers and paper-based shunts. Programmable flow delays offer an alternative method to geometry for fluid control. The wet-out through dry membrane can be slowed by pre-drying sugar solution onto the membrane. The presence of higher viscosity sugar solutions previously deposited onto paper significantly slows flow. The origin of the time delay is predicted to be due to the effect of viscosity on the wicking times described by the classic Lucas-Washburn Equation. The time delays are referred to as dissolvable sucrose barriers. Varying sucrose concentrations dried onto paper membranes create fluid delays between minutes to nearly an hour. Dissolution of the sucrose barriers is markedly complex and the wet-out path is highly variable. Nevertheless, the time delays are reproducible and have a tunable range that is appropriate for POC diagnostics, especially translation into 2DPNs.

Figure 11 shows a schematic of a 2PDN designed for the delivery of four fluids to a common detection region and the timed sequential delivery of the four fluids through the detection region.

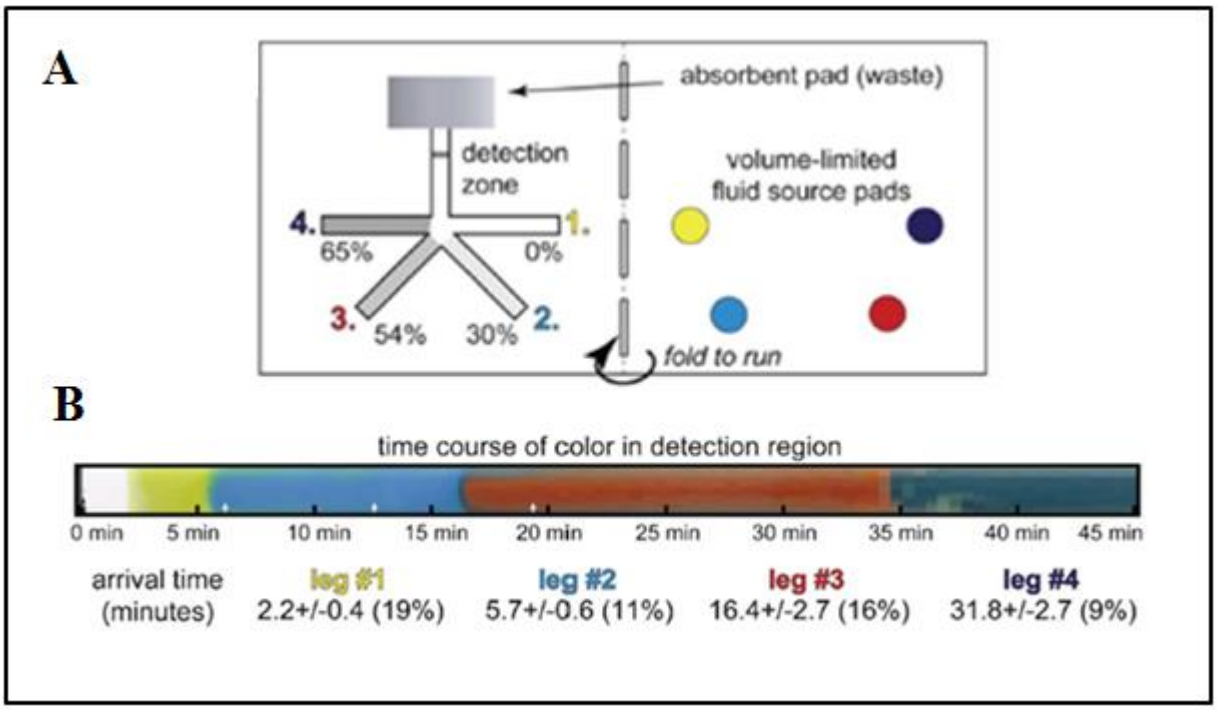

Figure 11. Schematic of a 2PDN card with dissolvable sucrose barriers. (A) Sugar solution is applied to each leg. 11 µl of dyed phosphate buffered saline with Tween-20 was added to the source pads on the right side of the card. Fluid flow is activated by folding the card. (B) Time course of color fluid through the detection region. The average arrival time of each fluid for N = 5 devices was calculated. Images were adapted from Lutz B, Liang, T et al [52].

For this particular design, the four fluids are of identical volumes. Glass fiber has a volume metering capability as previously described and was used as source pads in this 2PDN design. Fluid flow shuts off when the fluid source is depleted. The fluid flow from each leg of the device reaches the main channel at specific times dependent on the sugar delay. Higher concentration sugar delays translate to longer times between fluid activation and fluid reaching the detection zone. A multi-step assay for signal amplification was demonstrated using the malaria model system (Figure 12) in a 2PDN-based paper assay with dissolvable sucrose barriers.

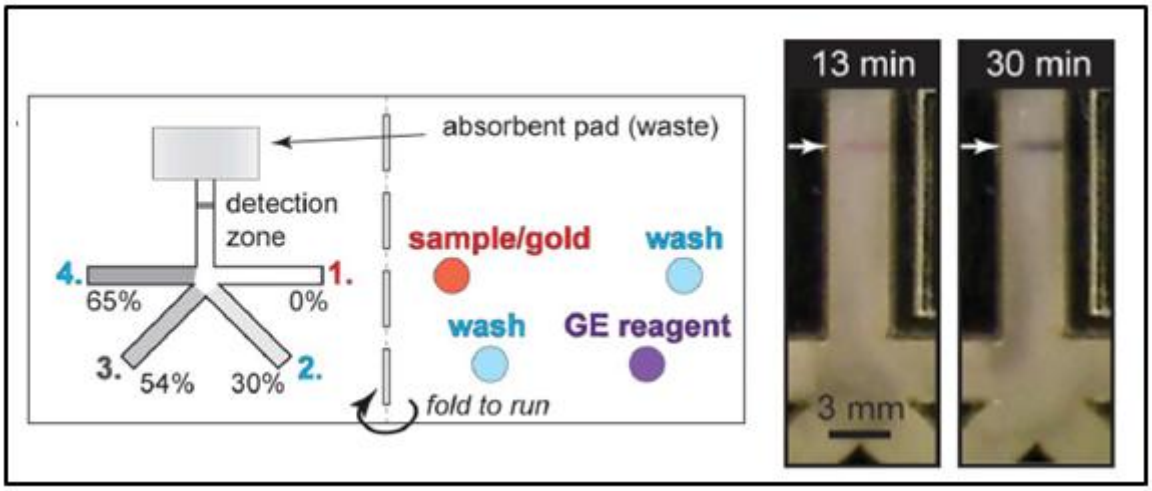

Figure 12. Schematic of a 2PDN-based multi-step assay with dissolvable sucrose barriers for malaria detection. (A) Sugar solution is applied to each leg. 11 µls of sample premixed with gold, TBST washes, and gold enhancement reagent were added to the source pads on the right side of the card. Fluid flow is activated by folding the card. (B) Image of the detection region at 13 minutes after the delivery of the first wash step and 30 minutes after the delivery of gold enhancement. White arrows mark the capture region where capture antibody was spotted. Images adapted from Lutz B, Liang T, et al. [52].

An enhancement of 2.6 fold was achieved, which is slightly less than the 4-fold gain in the 2DPN device shown in Figure 6. Limit of detection measurements, however, were not collected for this 2DPN card design. Relevant work on dissolvable sugar bridges [53] as an alternative tool for volume metering showed a negative effect of sugar on signal generation in the model system.

An alternative method to achieve flow delay is to divert fluid into an absorbent pad-based shunt placed in contact with the main membrane. Altering the length, thickness, and material of the shunt creates reproducible time delay that range from 3 to 20 minutes. Figure 13 outlines fluid flow through a channel of a porous membrane in the absence of a shunt and in the presence of a shunt (Figure 13A).

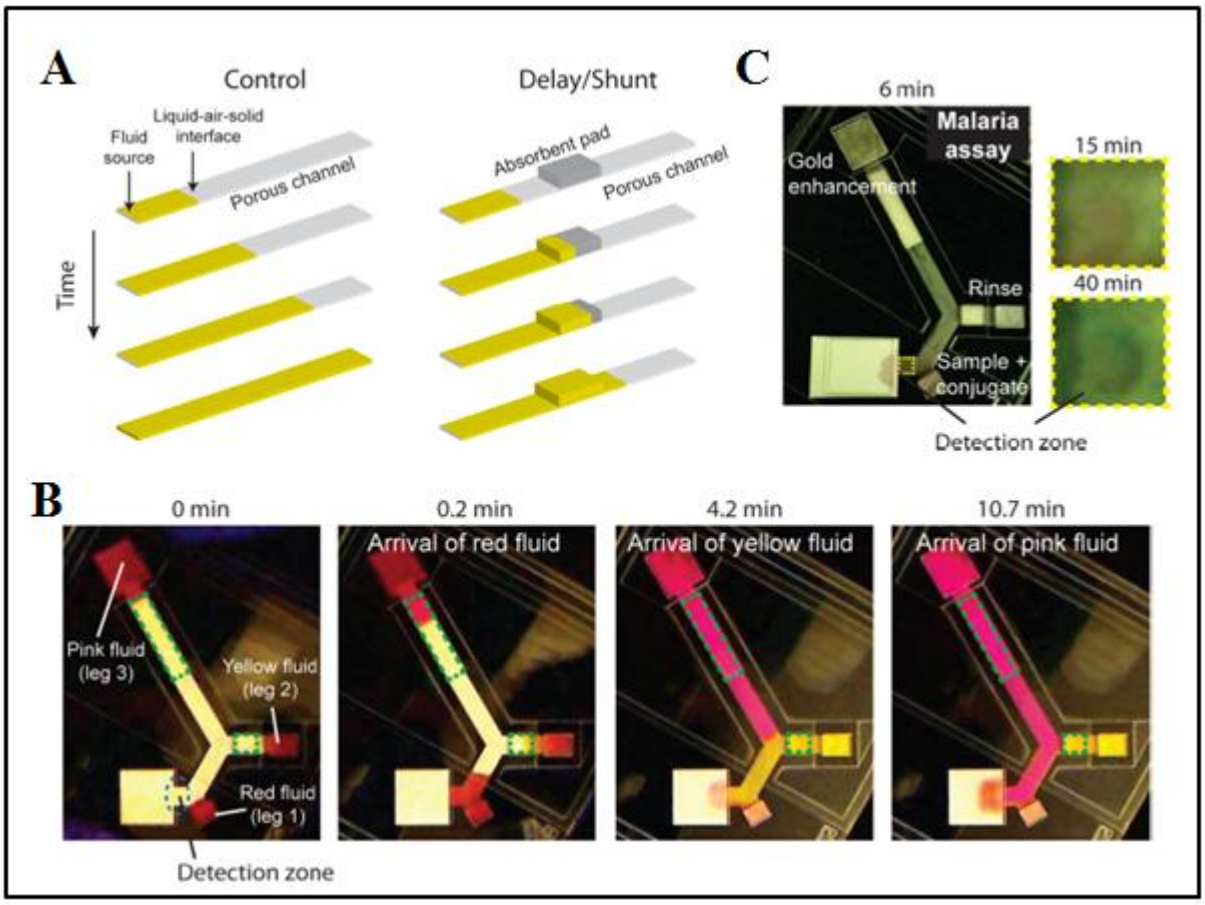

Figure 13. Sequential delivery of fluids using cellulose-delay shunts. (A) Fluid flow through a porous membrane in the absence of an absorbent cellulose pad shunt (left) and in the presence of an absorbent cellulose pad shunt (right). (B) Time-lapse images of a 2DPN folding card device for the sequential delivery of three colored fluids to a detection zone. The two shunts outlined by dotted green lines are made of cellulose of length 5.1 mm and 20.33 mm. (C) 2PDN folding card device demonstrating the amplified detection of malaria protein PfHRP2. Figure adapted from images by Toley et al [54].

Figure 13B shows sequential delivery of fluids in a 2PDN using shunts. A 2PDN with shunts carrying out a multi-step signal enhancement assay was demonstrated using the malaria model system (Figure 13C). The main advantage of the shunts as fluid delays is the reduction of paper network footprint and assay time. The shunts enable delivery of larger volumes of fluid to the detection region compared to the volumes of fluid delivered in the absence of a shunt. However,

a high volume of reagent must be retained in the shunts for the shunts to work. In the case of the 2DPN for malaria reagents were stored dry upstream of the shunts so the only fluid wasted was water. For reagents that either cannot be stored dried or require more expensive rehydration buffers, there is some waste produced by the shunt system.

3.6 Conclusions

Three different 2PDNs in the context of malarial antigen detection where presented in this chapter. Each carried out the same multi-step amplified assay using gold enhancement as the signal amplification reagent. Geometry, dissolvable sucrose barriers, and pad-based shunts are novel tools for the control of fluid flow in paper. Table 3 lists the advantages and disadvantages of the three fluid control tools presented in this chapter.

Table 3. Comparison of fluid control methods.

Fluid Control Method	Advantages	Disadvantages
Paper Network Geometry	• simple to fabricate	• Large device footprint • long time to result at high(er) reagent volumes
Dissolvable sucrose barriers	• potential to reduce device foot print • potential to reduce time to result compared to using geometry alone • inexpensive	• possible inhibitory effect of sucrose on signal generation • fabrication is more complex compared to geometry
Pad-based shunts	• potential to reduce device foot print • potential to reduce time to result compared to using geometry alone • relatively easy fabrication	• shunts retain fluid, so high(er) volume of reagents needed that will not reach detection region

Multiple 2PDNs were demonstrated in the context of malaria detection using a multi-step amplification assay. The fluid control tool kit consisting of paper network geometry, dissolvable

sucrose barriers, and cellulose-based delay shunts were demonstrated for their ability to enable sequential fluid delivery in 2PDNs. A total of three reagents were delivered sequentially to a detection region. Different chemical processes involving three reagents or more can be translated into 2PDNs. The multi-step signal amplification process was demonstrated within this chapter, but other multi-step processes can be translated as well. Of particular interest through the remainder of this thesis is whether decoupling the delivery of analyte and gold conjugate, delivered together in our multi-step amplified assay and conventional LFTs, can improve sensitivity. The following chapters investigate the potential gains in sensitivity between two delivery formats, premixed one step delivery and sequential delivery of analyte and colorimetric label, in the malaria system.

Chapter 4: Investigation of the format-dependent spatial distribution of binding

4.1 Objectives

Conventional LFTs (Figure 2) use a dry premix format for a rapid one step delivery of analyte and colorimetric label. As mentioned previously, the classic LFTs place a constraint on the complexity of the chemical processes carried out. For operation, the user typically adds sample (urine or a drop of blood) to the test. In the case of many commercial malarial LFTs, the user must also add drops of buffer that come with the test. The 2DPNs discussed in Chapter 3 were all examples where analyte and colorimetric label were delivered in one step. With 2PDNs, we can deliver the same premix format but at more controlled times and volumes of sample and wash buffer.

2DPNs allow multistep chemical processes to be carried out. One example of a multi-step chemical process is signal amplification, which was highlighted in Chapter 3. Another multi-step chemical process involves decoupling the delivery of the analyte and gold conjugate. Initial experimental results (Figure 14) show a striking difference in the signal intensity and spatial distribution of signal between the sequential and premix delivery formats.

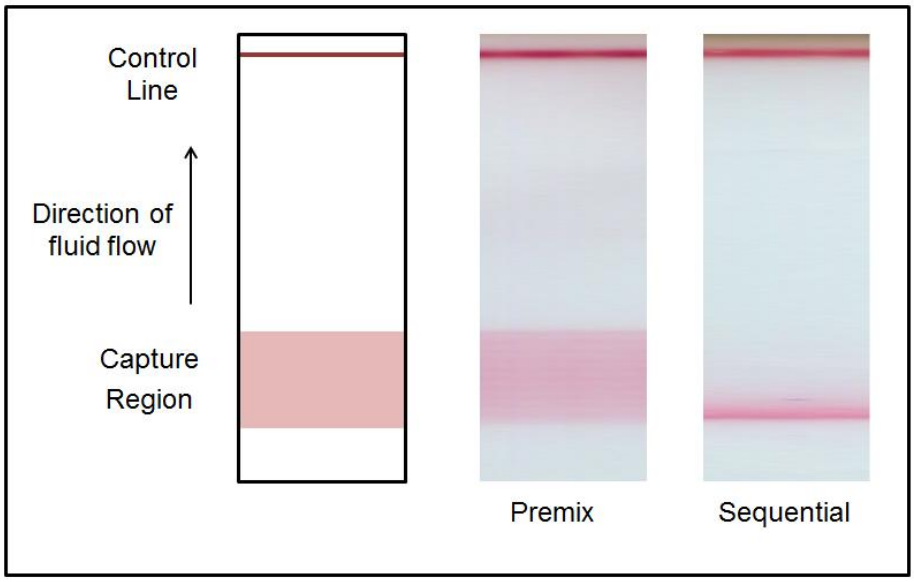

Figure 14. Premix (middle) and sequential (right) generated signal. Schematic of membrane indicating location of capture region and control line (left). The sequential and premix signals have distinct characteristics.

The spatial distribution of binding between the premix and sequential delivery formats is visibly very distinct. In the premix case, the signal intensity is uniformly distributed along the entire length of the capture region; in the sequential case, a high intensity upstream binding edge appears.

It is predicted that the differences in the spatial distribution of binding is the direct result of the binding kinetics of the malaria system used. The objective of this chapter is to present a set of experimental results to support the hypothesis that the specific binding kinetics of the malaria system results in the different binding patterns seen.

4.2 Binding Kinetics and Diffusion

The assay signal seen in a colorimetric-based assay is the direct result of binding events that occur at the capture region. In traditional sandwich assays, there is typically a single antibody

conjugated to the colorimetric label and a single epitope on the analyte that binds to the paratope on the capture antibody. There are four binding events of importance in a typical sandwich assay: 1) analyte binding to the capture antibody, 2) antibody with colorimetric label binding to an analyte bound to the capture antibody, 3) analyte bound to the antibody with colorimetric label binding to the capture antibody, and 4) analyte binding to the colorimetric label. The relative binding rates of the binding events can guide the determination of the appropriate reagent delivery method to achieve the highest sensitivity.

Binding parameters of importance are specifically the kinetic rates and protein concentrations. A low dissociation constant (K_d), a ratio of dissociation (k_{off}) and association (k_{on}), for the antibody-antigen interaction is ideal for immunoassay design. First-order rate equation describing the binding kinetics between two interacting species A and B forming complex AB follows:

$$\frac{d[AB]}{dt} = k_{on}[A][B] - k_{off}[AB]$$

For the malaria PfHRP2 system, the binding of a myriad of complexes to the capture antibody patterned at the capture region will contribute to the signal produced. The PfHRP2 analyte has 18 conserved epitopes. The 40 nm gold nanoparticle is conjugated to approximately 12 IgGs, which translates to 24 possible binding sites. Due to steric constraints, it is highly unlikely for all 24 binding sites to be bound to an analyte at a given time. However, a single gold nanoparticle decorated with IgGs is likely to be covered by multiple analyte molecules simultaneously (Figure 15B). A double gold-complex (Figure 15C) is also possible, where two gold nanoparticles are bridged by a single analyte. Higher order complexes consisting of more than two gold nanoparticles are plausible.

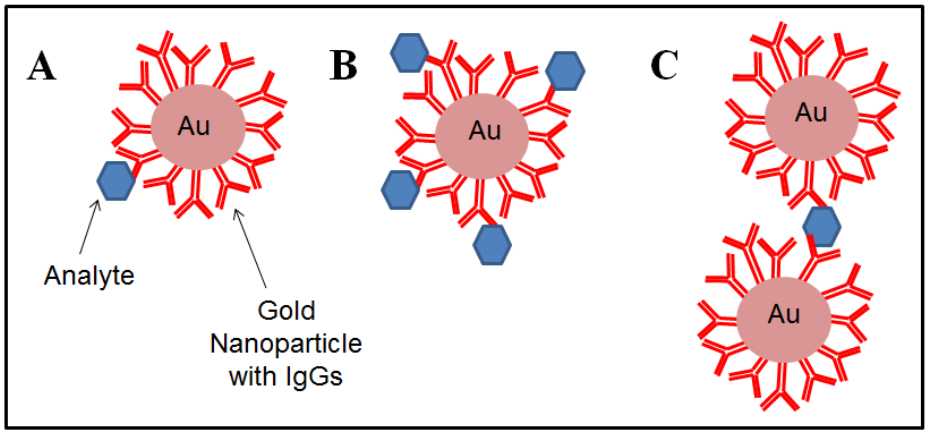

Figure 15. Schematic of a subset of complexes that can form. (A) Gold nanoparticle decorated with IgGs binds to analyte. (B) A single gold nanoparticle is bound to multiple analyte via the IgGs on its surface. (C) An analyte binds to two IgGs on different gold nanoparticles; this is referred to as a double-gold complex.

Due to the number of binding sites on both protein of interest and gold nanoparticle coated with IgGs, avidity, also known as functional affinity, factors into the binding kinetics of the system. Avidity refers to the strength of multiple affinities of, in this case, a protein receptor binding to an antibody. A molecule with 10 binding sites has a higher avidity compared to a molecule with 2 binding sites for the same protein of interest assuming comparable binding affinities.

The sizes of these complexes and lone analyte differ in size, affecting the effective diffusion of these complexes and lone analyte. Molecular diffusion plays an important role in reagent transport. The random Brownian motion of particles results in molecular diffusion. The diffusivity, D, of a molecule can be approximated by the Stokes-Einstein equation:

$$D = \frac{k_B T}{6\pi\mu a}$$

where k_B is Boltzmann's constant, T is temperature, a is the particle radius, and μ is viscosity. According to the equation, smaller complexes (small a) have a higher diffusivity compared to larger complexes (higher a) with all else being constant. In the PfHRP2 system, the diffusivity of

the PfHRP2 analyte using the viscosity of water at room temperature is approximated to around 2.5 x 10^{-10} m^2/s. The diffusivity of a PfHRP2 analyte bound to a 40 nm gold nanoparticle by the surface IgG is approximated to around 1 x 10^{-11} m^2/s. There is an approximated 25 fold difference in diffusivity of a single PfHRP2 analyte compared to a PfHRP2 bound to a 40 nm gold label. The analyte and analyte-gold conjugate complexes in porous media are also carried by the dynamic fluid flow.

4.3 Investigation of Sequential and Premix Distribution of Binding Results

4.3.1 Introduction

The sharp upstream binding pattern for sequential and uniform binding pattern for premix suggests the affinity for the capture pfHRP2 monoclonal IgM is higher for the lone pfHRP2 compared to the affinity of capture pfHRP2 monoclonal IgM to a complexed species (Figure 16).

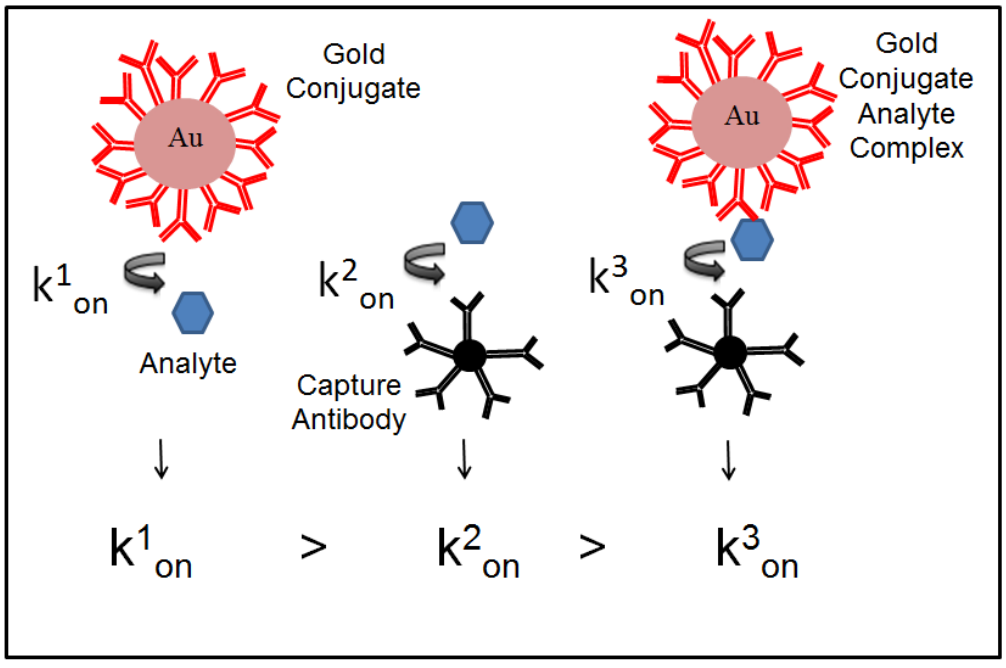

Figure 16. Illustration of binding events and the predicted relationship between the rate constants.

A lone PfHRP2 molecule diffuses much faster than any complexed species due to size based on the Stokes-Einstein equation. As lone PfHRP2 molecules approach the capture region, it binds to the capture IgM and the concentration of the lone PfHRP2 depletes in solution as the solution continues to flow through the capture region. A lone PfHRP2 molecule with nothing decorating its surface has more rotational freedom than a PfHRP2 molecule bound to a 40 nm gold nanoparticle with its IgGs. The greater rotational freedom gives the lone PfHRP2 an advantage in positioning for capture by the capture IgM. It is predicted that a double gold-complex and higher order gold complexes will have a lower probability of binding to the IgM compared to an analyte bound to an IgG on a gold nanoparticle and a lone analyte molecule.

To investigate whether the distinct binding patterns seen was the direct result of the differences in binding kinetics predicted of the different complexes and lone PfHRP2 in the multivalent system, premix assays were run with varying optical densities of gold conjugate then followed by the addition of a pure high gold conjugate solution. By varying the optical density of the gold conjugate solution, the concentration of IgGs, which are conjugated to the surface of the gold nanoparticles, varies. The formation of complexes is dependent on both the concentration of the IgGs and the PfHRP2 analyte. With lower IgG concentration, the formation of complexes is expected to decrease. Adding the pure gold conjugate solution allows a visual confirmation of where and if there is available PfHRP2 to be bound.

4.3.2 Methods

Membrane and Reagent Preparations

Capture antibody was patterned at 1 mg/ml with a piezoelectric inkjet printer to create a capture patch 3 mm wide by 2.5 mm in length on a nitrocellulose membrane (HF135, Millipore,

Billerica, MA) strip 3 mm wide by 30 mm in length. An anti-mouse antibody was printed at 0.5 mg/ml for a control line 3 mm wide by 0.25 mm 8 mm upstream of the capture patch. Membranes were placed in a 37 ºC oven for 2 hours and then stored in a desiccator. Printed membranes were blocked the day following printing in 5 % sucrose, 2.5 % polyvinylpyrrolidone (PVP), 2.5 % bovine albumin serum, and 0.1 % Tween-20 in phosphate buffer saline blocking solution to minimize nonspecific absorption. Glass fiber pads were cut on the CO_2 laser subsequently washed three times with deionized water, and then dried in a 37 ºC oven overnight.

Known concentrations of the recombinant malaria protein PfHRP2 was spiked into fetal bovine serum to serve as a mock sample solution. TBST (TBS with 0.1 % Tween-20) was used as both the wet-out and wash buffers. An OD 5 gold conjugate solution was made up of five parts of gold conjugate at OD 10.2, four parts TBS, and one part TBS with 1 % BSA solution. A premixed solution consisting of five parts gold conjugate at OD 10.2, one part TBS/BSA solution with 1 % BSA, and four parts mock sample was mixed immediately prior to assay application. Six different premixed solutions were made so the final ODs of the gold were 5, 1, 0.5, 0.1, 0.01, and 0. Gold conjugate were serially diluted in TBS from the starting OD of 10.2.

Experimental Protocol

Six assays were run in each set simultaneously with OD 5, 1 0.5, 0.1, 0.01, and 0 premix solutions at 20 ng/ml. A set was run four times, but due to assay running errors, OD 5 had only 3 replicates and OD 0 had only 2 replicates. 30 µl of premixed sample and gold conjugate was added to 7 mm by 7 mm source pads. At 7 minutes, the source pads were washed with 10 µl of TBST. At 9 minutes, the source pads were swapped out for 8 mm by 8 mm source pads and 40 µl of TBST was added. The assays were scanned at 17 minutes. At 19 minutes 40 µl of OD 5

gold conjugate solution was added followed by a 10 µl of TBST at 28 minutes to rinse out remaining gold conjugate in the source pads. The source pads were swapped at 30 minutes and 40 µl of TBST added. The membranes were scanned at 40 minutes.

Image Acquisition and Analysis

A high resolution-scanner (Epson, Nagano, Japan) was used to acquire image data at 1200 dpi at 17 minutes (after just premix gold application) and at 40 minutes (after OD 5 gold application). The images were processed using a custom Matlab program by Robert Robinson at Oregon State University to create line profiles of the signal intensity across the capture region in the direction of fluid flow.

4.3.3 Results

Premix assays were run at varying gold conjugate ODs starting at OD 5 down to OD 0 (no gold conjugate). The assays were scanned after the addition of the premix sample solution and a wash. The assays run with an OD 0.1 premix solution showed the uniform binding characteristic of the premix delivery format but unlike at the higher OD premix solutions the binding is not along the entire capture region. At OD 0.5 and OD 1 premix solutions, there is binding along the entire capture region, but the intensity of the binding at the upstream edge appears to be higher compared to the rest of the capture region (Figure 17A).

To determine whether and where there was available PfHRP2 analyte bound at the capture region, an OD 5 gold conjugate solution was then added to the membranes. As expected, the no gold conjugate (OD 0) has the distinct sequential binding pattern seen previously. With the addition of excess gold conjugate solution, a higher intensity binding pattern at the upstream

capture region is seen in the OD 1, 0.5, and 0.1 premix solution assays compared to prior to the addition of the OD 5 gold conjugate solution. The OD 5 premix solution assay shows the same uniform binding throughout the capture region seen prior to the addition of the OD 5 gold conjugate solution (Figure 17B).

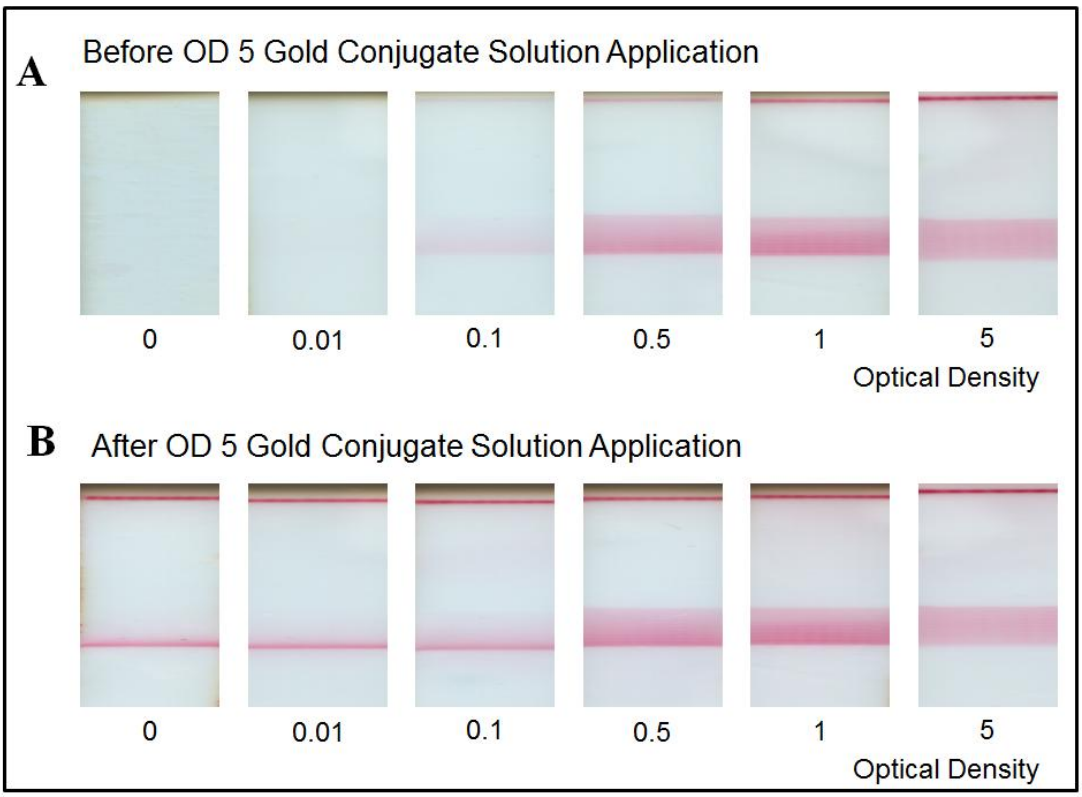

Figure 17. Images of the assays at OD 5, 1, 0.5, 0.1, 0.01, and 0 premix solutions at a PfHRP2 analyte concentration of 20 ng/ml. (A) Representative images after addition of the premix sample and a wash step. (B) Representative images after the OD 5 gold conjugate solutions followed by a wash step.

The grayscale signal intensity across the length of the capture region in the direction of flow was found using a custom Matlab program. The line profiles show uniform signal intensity along the capture region for OD 5. The uniformity of the line profile decreases as the OD of the gold conjugate premix solution decreases (Figure 18A). The OD 5 gold conjugate application resulted

in high intensity binding at the upstream capture region for all the OD premix solutions except OD 5.

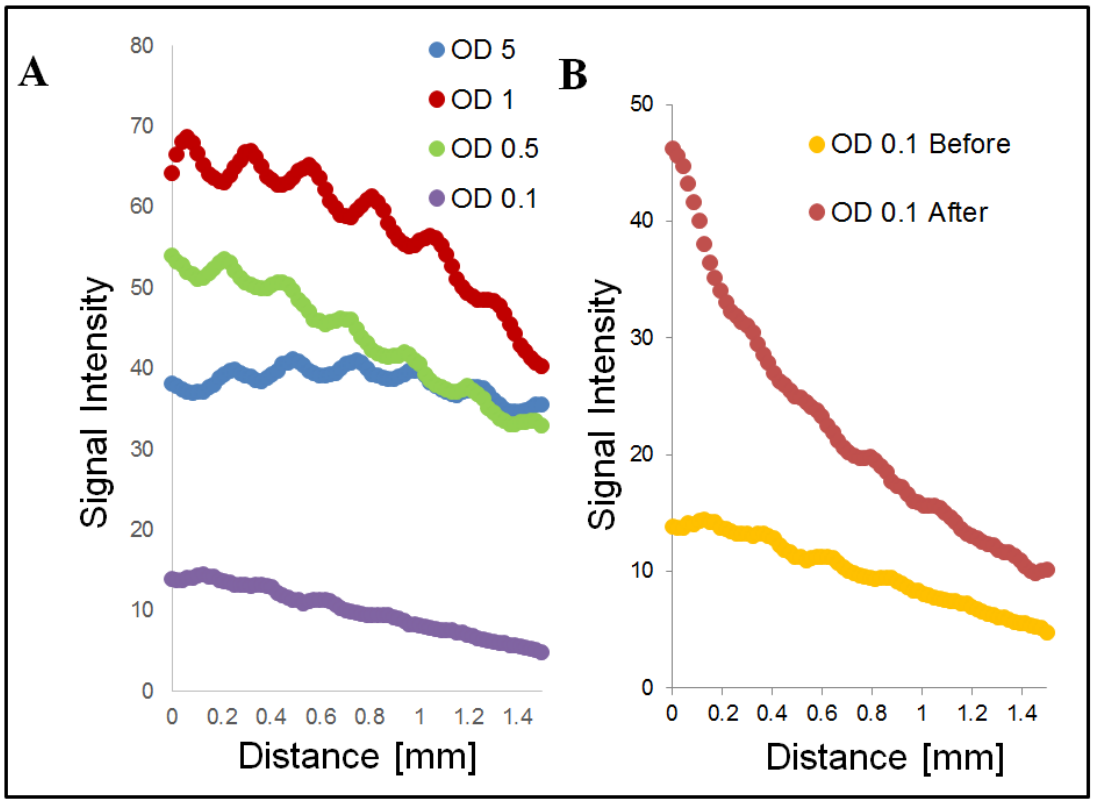

Figure 18. Signal intensity profiles along the capture region. (A) Signal intensity profiles along the capture region prior to OD 5 gold conjugate application for OD 5, 1, 0.5, and 0.1 premix solutions. (B) Profiles of OD 0.1 premix solution before and after OD 5 gold conjugate application.

4.3.4 Discussion

The results of the experimental data suggest that the formation of complexes results in the more uniform binding pattern characteristic of the premix delivery format. The binding of lone PfHRP2 to the capture IgM patterned at the capture region followed by the binding of IgG on the surface of gold nanoparticle results in the high intensity upstream binding pattern characteristic of the sequential delivery format. The trends from the experimental data are consistent with the predicted rate constant trend illustrated in Figure 16.

The decreasing uniformity of the binding pattern seen with decreasing OD of the premix solution is likely the result of the decrease in the concentration of gold nanoparticles and thus the concentration of IgGs in solution available to bind to the PfHRP2 molecule. As the probability of forming complexes decreases with decreasing OD, the spatial distribution of the binding pattern begins to resemble the sequential delivery format. As the concentration of IgGs decreases, the premix solution contains lone PfHRP2 and PfHRP2 bound to gold conjugate. The lone PfHRP2 in this case is expected to behave as free PfHRP2 in the sequential case and bind to the upstream edge of the capture region. The addition of the pure gold conjugate solution shows the appearance of high intensity binding at the upstream edge of the capture region confirming the prediction. The increase in signal intensity along the upstream edge at the lower OD premix concentrations after OD 5 gold conjugate solution addition indicates free PfHRP2 in solution preferentially binds to the upstream edge of the capture region, a result of the higher effective diffusivity of free PfHRP2.

Any analyte with an epitope available for binding captured at the capture region can still bind to the IgG conjugated to the gold nanoparticle. The absence of an increase in signal intensity and preservation of uniform binding in the capture region with the addition of OD 5 gold conjugate solution to the OD 5 premix solution assays indicates little surface binding of the gold conjugate at the capture region. Possible explanations for this are the surface binding of the gold conjugate is sterically hindered or the affinity between the IgG conjugated to a gold nanoparticle is low for a PfHRP2 molecule already bound to another IgG conjugated to a gold nanoparticle.

The k_{on} for the binding of gold conjugate to the analyte was measured via SPR experiments to be approximately 2 $x10^6$ $M*s^{-1}$ and 1 $x10^6$ $M*s^{-1}$ for the binding of analyte to the IgM capture

antibody (data courtesy of Jared Houghtaling). The measured k_{on} values agree with our initial prediction and experimental results.

4.3.5 Conclusions

The experimental results confirm the binding kinetics of the multivalent system play in important role in the spatial distribution of binding patterns seen in the premix and sequential delivery format cases. In the malaria PfHRP2 system, experimental results and SPR results courtesy of other members of the lab support our initial prediction that of four binding pairs considered the following is true: 1) the affinity of analyte to an IgG on the gold nanoparticle is the highest of the binding pairs, 2) the affinity of analyte to the IgM capture antibody is lower and comparable to the affinity of an IgG on a gold nanoparticle to an analyte bound to the IgM (Figure 16). The result of the differences in binding kinetics is very distinct binding profiles. The impact of the distinct binding profiles on the assay sensitivity will be investigated in Chapter 6. The following chapter, Chapter 5, describes the development of assay protocols for determining limits of detection for both the premix and sequential delivery formats.

Chapter 5: Development of Premix and Sequential Assay Protocols

5.1 Objectives

The experimental results presented in Chapter 4 motivated the investigation of the possible gains in sensitivity from decoupling the analyte and gold conjugate delivery over the conventional premix format. The purpose of this chapter is to develop manual protocols, where reagents are added to glass fiber source pads and flow initiated manually at specified times for both the premix and sequential delivery formats. The minimum number of assay steps for the sequential delivery format was determined based on the spatial binding distribution through the test line region and background analysis.

5.2 Development of a Premix Format Assay Protocol

5.2.1 Introduction

A manual premix protocol was developed for determining the limit of detection in a premix delivery format. A card device to carry out four assays in parallel was designed. Several factors of importance considered in the development of such a protocol and device include: timing of reagent delivery and reproducibility. The manual delivery of reagents at predetermined times allows us to collect useful information on assay sensitivity prior to the design of a 2DPN. The information collected with regard to timing and reproducibility provide guidelines for the rationale design of an automated 2DPN.

Timed Delivery

The idea of fluid activation by folding allows for the running of multiple assays side by side with the synced delivery of reagents. The reagent can be loaded into several separate source pads and

activated by a simple folding step to run multiple assays in parallel. The source pads are composed of glass fiber, which have a volume metering capability discussed in Chapter 3.4. Briefly, glass fiber pads show reproducible fluid release from pads of varying fluid capacities. Comparison of wicking fluid into nitrocellulose strips from different source materials (nitrocellulose, cellulose, and glass fiber) showed glass fiber was the only source material that completely drained its fluid content [36]. The appropriate times for adding each subsequent reagent was found based on a combination of factors: visual interpretation of contents remaining in the source pad at specific time points, calculated volume remaining in source pads after removal at specific time points, and the uniformity of the fluid front of the subsequent reagent.

Reproducibility

The device fabrication methods described in Chapter 3.3 enables improvement over our previous assay protocol, where membranes were adhered to a plastic card and flow relied on the continued contact between the membrane and source pad with no applied pressure (Figure 19).

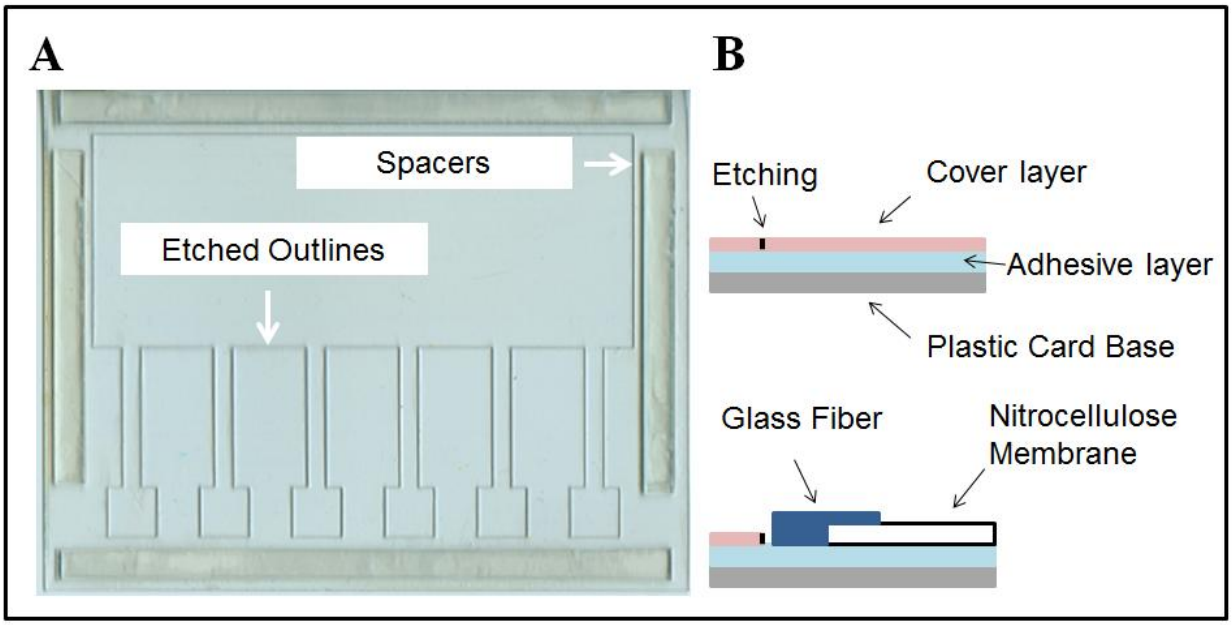

Figure 19. Simple plastic card for running assays. (A) Image of typical plastic card base for running six assays. The card base is made of 10 mil plastic with an adhesive layer and cover layer. Spacers prevent the membranes from touching the surface bed of the scanner, preventing damage to the membranes. Etched outlines cut only through the cover layer using CO_2 laser settings outlined in Chapter 3.3. (B) Side view schematic of the plastic card at the membrane to glass fiber contact point without membrane and glass fiber (top) and with membrane and glass fiber (bottom). The cover layer is removed to expose the adhesive layer, which holds the membrane and glass fiber components in place.

The irreproducibility of membrane to source pad contact was hypothesized to result in the high deviations in mean signal intensity seen in some of our experimental results. Inconsistent membrane to source pad contact between each assay influences flow of reagents, reagent interaction times, and thus differences in signal intensities at the same analyte concentration. High variability greatly reduces assay accuracy. New fabrication methods allow for the incorporation of adhesive layers, which can provide external pressure to maintain membrane to source pad contact. Adhesive layers were incorporated into a card device to run multiple assays in parallel. Colored dyes were used to investigate the uniformity of the fluid front approaching the capture antibody region (test line region) in the designed card devices.

Another hypothesis for the source of high variability was the uneven coating of the membranes during the blocking process to reduce nonspecific protein absorption. Such uneven coating of the membrane with proteins and sugars may result in non-uniform fluid fronts. Non-uniform fluid fronts attribute to differences in reagent flow between assays. A small sample wet-out buffer prior to the addition of sample was investigated as a method to remove this uneven coating that may have results from the blocking process.

5.2.2 Methods

Volume Release by Membrane to Pad Contact Method Experiments

The volume release profile over time for source pads in contact with membrane with no external pressure and with external pressure applied were determined. Membranes were fully-wetted out with yellow colored fluid. 30 µl of colored fluid was added to 7 mm by 7 mm glass fiber pads in contact with a 3 mm wide by 120 mm in length membrane. 40 µl of colored fluid added to 8 mm by 8mm glass fiber pads in contact with a 3 mm wide by 140 mm in length membrane. Five membranes were tested at each volume with external pressure and without external pressure applied to the membrane to source pad contact point. The volume released from the source pads was calculated using the following formula:

$$V(t) = A(t) * h * p$$

where V(t) is volume as a function of time, A (t) is area as a function of time, h is membrane height (~ 135 µm), and p is porosity (~ 0.8). The height and porosity values are reported values published by the manufacturer. The area was calculated by finding the distance the fluid front travelled at each time point in ImageJ (U.S. National Institutes of Health, Bethesda, MD [55]) and multiplying by the width of the strip (3 mm).

Card Design and Fabrication

An initial card design was drafted using AutoCAD (Autodesk, San Rafael, CA). The initial card design took into consideration that the membrane should not touch anything on the folding portion of the card except the glass fiber source pads. Glass fiber source pads were elevated with various thicknesses of adhesive pieces to ensure contact with the membrane after folding. Cards were cut using a CO_2 laser using the specific cutting parameters outlined in Chapter 3.3. Card designs were tested for uniform fluid delivery and contact using colored fluids and modifications

were made based on the results. For the final card design, the user activates fluid flow by folding over the appropriate portions of the card.

Image Acquisition

Yellow and red food coloring was added to deionized water to create three distinguishable color solutions of yellow, orange, and red. A 2 mM eriogluacine blue solution was made in lieu of a solution of blue food coloring in deionized water due to chromatographic effects. The colored solutions were used to visualize fluid flow in the card design. A high resolution-scanner (Epson, Nagano, Japan) was used again to acquire image data at 300 dpi at various time points.

5.2.3 Results

Previous assays described were run on a simple piece of plastic with scoring to help with alignment of the assay components (Figure 19). The card shown in Figure 20 has several modifications including: spacer pieces for external pressure to maintain membrane to source pad contact, multiple folds for multiple synced fluid application steps, and larger source pads to prevent fluid pooling due to the added external pressure.

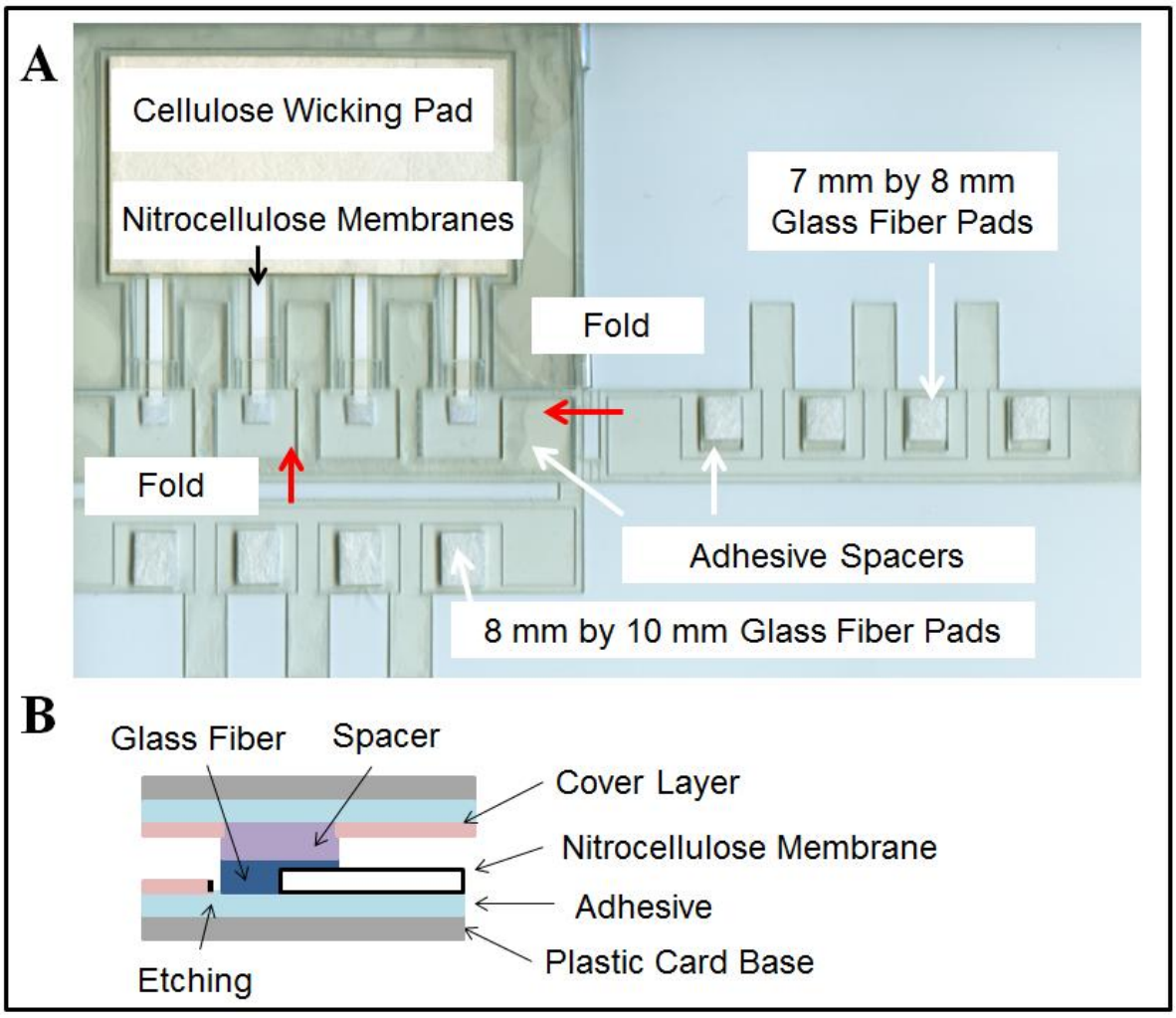

Figure 20. Manual Format Card Design. (A) Image of manual format card design with the components with the main components labeled. There are two folding portions. The directions of the folds are indicated by the red arrows. Adhesive spacers are used to apply external pressure at the membrane-glass fiber pad contact points and to hold the folds in place. (B) Side view schematic of the manual format card at the membrane-source pad contact point. The spacer adds external pressure at the membrane-source pad contact point. The spacer is made of two pieces of 10 mil plastic with an adhesive and cover layer sandwiched together. It has adhesive on both sides for attaching the glass fiber source pads and adhering to the plastic card base.

Colored fluids were used for visual interpretation of the uniformity of the fluid fronts after each fluid activation step via a card folding step. A comparison of the volume of fluid released with

the adhesive pieces for external pressure and without the adhesive pieces for 30 µl and 40 µl fluid volumes showed little difference in the volume release versus time profile (Figure 21).

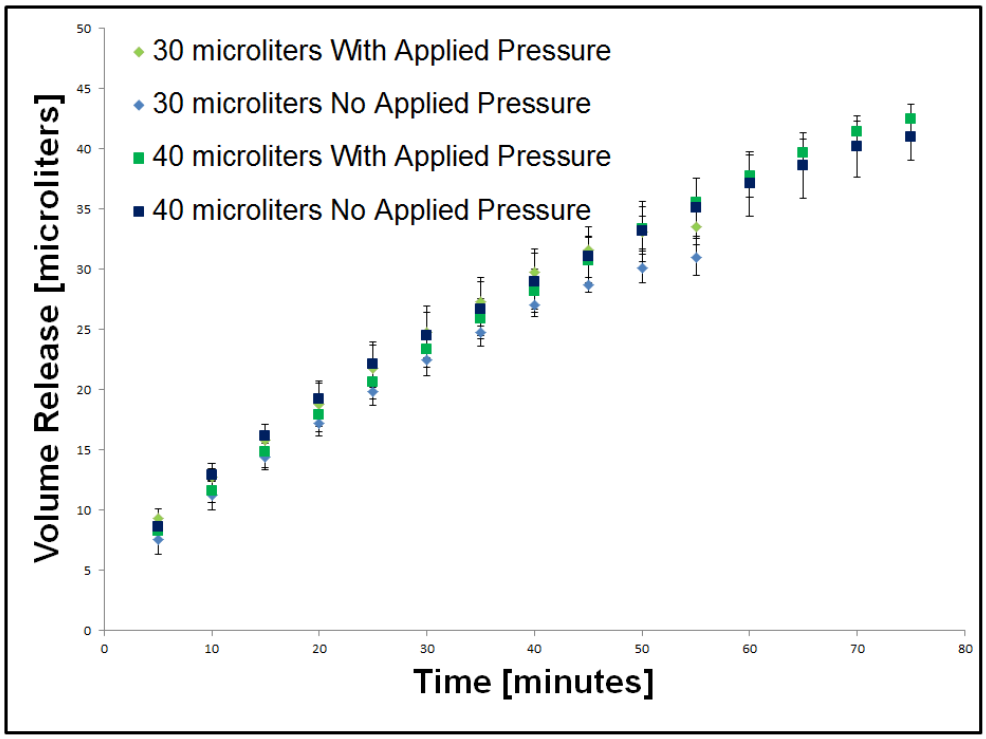

Figure 21. Volume release from glass fiber source pads with applied pressure and without applied pressure. The plot shows the volume released from glass fiber source pads for source pads with applied pressure at the membrane source pad contact point and no applied pressure at the membrane source pad contact pad. Each data point is the average of 6 measurements (with applied pressure), 4 measurements (30 µl no applied pressure), and 3 measurements (40 µl no applied pressure). Error bars represent the standard deviation.

With the previous assay, the sample solution was first added to a dry membrane and followed Washburn flow. After wet-out of the membrane, this was calculated to take approximately 9.72 µl, the remaining sample volume and each subsequent reagent delivered followed Darcy flow. A visual of the wet-out of a dry membrane previously blocked in our low bovine albumin based blocking solution shows a non-uniform fluid front. Red colored fluid added to the same membrane now fully wetted out showed a uniform fluid front. The results suggesting a wet-out

of the membrane prior to sample application helps the uniform delivery of detection solutions prompted the inclusion of a membrane wet-out step consisting of a 10 µl wet-out solution via a 5 mm by 5 mm glass fiber pad.

Colored fluid was run in the card (Figure 20) to mimic the 10 µl wet-out solution (yellow), 30 µl premixed sample solution (orange), 40 µl wash solution (red), and 40 µl enhancement solution (blue). The same glass fiber source pads sizes and timing used in the previous assays described was tested. Due to the applied pressure from the adhesive spacer pieces, it was found that the fluids would pool when the source pads initially contact the membrane, resulting in non-uniform fluid fronts and messy fluid delivery. The card was retested using 8 mm by 7 mm glass fiber pads for 30 µl volumes and 8 mm by 10 mm glass fiber pads for the 40 µl volumes. Due to the introduction of the 10 µl wet-out prior to sample application, the original assay protocol times for reagent application were modified based on visual interpretation of fluid release from the glass fiber source pads. An 8 mm by 10 mm glass fiber pad filled with 40 µl of red dye (Figure 22), the same size glass fiber pad 6 minutes after initial contact with the membrane, 13 minutes after initial contact, and glass fiber pad with no fluid added are presented to illustrate the visual differences between a glass fiber pad with fluid remaining and without nominal to no fluid remaining.

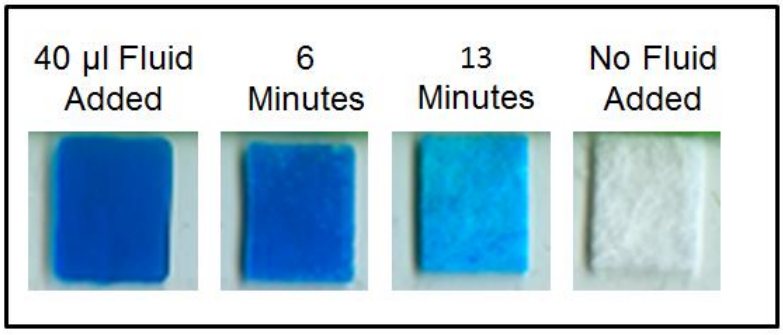

Figure 22. Glass fiber pads with different fluid volumes. Four 8 mm by 10 mm glass fiber pads were scanned directly after adding 40 µl of blue dye to the pad, six minutes after initiating fluid release from the pad, thirteen minutes after initiating fluid release from the pad, and when no fluid was added to the pad. At 13 minutes there is approximately less than 1 µl of fluid left in the glass fiber pad. The pad is still blue but has a similar textural gradient to as the source pad to which no fluid has been added.

Six 8 mm by 10 mm glass fiber pads were also weighed 12 minutes after initial contact. Using the density of water, the average fluid volume remaining in the glass fiber pads after 12 minutes was calculated to be 0.93 µl ± 0.94 µl.

From previous experiments it was noted that after the delivery of the premixed sample solution the pads retain a slight pinkish color, suggesting reagent release from the glass fiber pads is not perfect. Adding wash buffer directly to the same source pad resulted in an ineffective wash step due to the wash mixing with the residual reagent volume in the source pads. The effectiveness of a small volume rinse of the pads in reducing the mixing of reagents delivered via the same source pad was investigated. A 10 µl rinse of TBST (clear) was introduced to an 8 mm by 7 mm glass fiber pad 10 minutes after a 30 µl of yellow fluid was introduced. The TBST rinse pushed the yellow dye remaining the source pads after fluid release to the edges of the source pad (Figure 23).

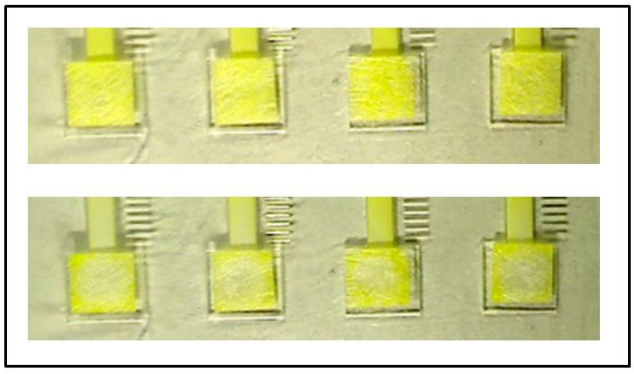

Figure 23. Four glass fiber pads prior to 10 µl TBST rinse (top) and after 10 µl TBST rinse (bottom). Previous fluid introduced to the glass fiber pads was yellow. TBST is a clear wash buffer.

Colored fluid was run in a card to determine the fluid delivery using the running protocol detailed in Table 4.

Table 4. Running protocol for premix delivery.

Step	**Time [min]**
10 µl TBST	0
30 µl Premix Sample	4
Swap Pads	13
40 µl TBST	14
Swap Pads	28
Scan	29
40 µl GE	30
Scan	40

Reagent activation steps via a fold in the card occur at 4 minutes for a 30 µl orange solution (premixed sample), at 14 minutes for a 40 µl red solution (wash) , and at 30 minutes for a 40 µl blue solution (gold enhancement). The timing of the fluid activation steps was determined based on visual inspection of the fluid release from the source pads and the approximately one minute time required to switch out the source pads. The fluid fronts are uniform as they approach the test line region of the strips after each of the fluid activation steps. The distance travelled by the fluid fronts is consistent across all four strips.

5.2.4 Discussion

The high variation in normalized signal intensities for the same analyte concentration seen in previous experimental results suggested a variation in fluid flow between strips. It was hypothesized that there was inconsistent source pad to membrane contact and the introduction of

an external pressure via adhesive pieces would help maintain source pad to membrane contact. The volume release versus time profiles of 30 µl and 40 µl fluid volumes under Washburn flow in a long strip of membrane showed similar release profiles. Although this particular set-up of wet-out in a long strip of membrane does not mimic the fluid flow in an actual assay, it provides information of the volume and fluid release over time. With the release profiles being very similar, the reproducibility issues previously seen are not expected to be related to variability in source pad to membrane contact. The existence of adhesive pieces for the application of external pressure, while not necessary, adds the ability to sync the timing of reagent applications to all four strips without the requirement for a multi-pipette. For this reason, the adhesive pieces and folding application was kept for the final card design.

The initial fluid introduced to a dry membrane previously blocked in a low BSA blocking solution showed non-uniform fluid fronts. Subsequent fluids added and exhibiting Darcy flow showed uniform fluid fronts. In previous assays, the initial fluid introduced to a dry membrane and exhibiting Washburn flow was the premixed sample solution. Non-uniform fluid flow of a premixed sample solution through the test line region directly influences the consistency of the interaction time between the analyte-antibody conjugated to gold nanoparticle complex to the capture antibody patterned at the test line. It is hypothesized that the non-uniform fluid flow is the result of the blocking proteins unevenly coating the membrane after the blocking process. The initial wet-out removes these residual proteins resulting in the uniform fluid fronts seen in the subsequent fluid addition. A 10 µl wet-out of TBST was incorporated into the assay protocol. TBST was chosen as the wet-out solution to match the wash buffer.

The time each reagent is introduced changes the volume delivered of the previous reagent as well as the uniformity of fluid flow. It was noted in previous experiments, not shown, that adding a new reagent when the previous reagent was not fully released from the source pad resulted in fluid pooling near the source pad. The appropriate reagent application times were found based on visual analysis of the source pads. The residual volume was calculated to support our visual analysis. The residual volume remaining in the source pads were calculated at the 12 minutes and found to be close to minimal (~ 1 µl). The large standard deviation is expected due to the low accuracy of the balance. For the 30 µl and 40 µl volumes, 9 minutes and 13 minutes, respectively, were found to be the ideal time point where the majority of the 30 µl volume is released and the addition of a new fluid would result in little pooling.

Swapping the pads between reagents was found to be important in reducing the mixing of reagents in the source pad prior to flow through. A rinse of pad failed to push residual reagent out of the source pad and through to the membrane. The residual reagent instead accumulated at the edges of the source pads. This has implications on our paper network design. It is important to consider the interactions of reagents flowing through the same source pads. The selection to switch out source pads between reagents suggests that introduction of reagents through different paths in a paper network design may be advantageous for reducing unwanted reagent interaction prior to reaching the test line.

A complete assay protocol for premix delivery was developed and presented in Table 4. The plastic card housing was tested with colored fluids to illustrate the fluid delivery. Uniform fluid fronts are demonstrated. The distance the fluid front travels is also consistent between the four strips in each card.

5.2.5 Conclusion

There were two main objectives: 1) develop a manual premix assay protocol and 2) design a plastic card to run multiple assays simultaneously with consistent fluid delivery. With respect to the first objective, appropriate reagent application times were determined. Switching out pads was determined to be necessary to reduce unwanted reagent interactions prior to flowing through the test line region. Reagent flow in a fully wetted out membrane was found to have more uniform fluid fronts than a dry membrane previously blocked in a low BSA blocking solution. The findings of this section have several implications for paper network design. Design consideration should be given to any reagent interactions that may occur in areas where the fluid flow paths intersect. An initial wet-out fluid is required to maintain uniform fluid delivery in the blocked membranes used. With regards to the second objective, the card shown in Figure 16 allows for the synced introduction of reagents through folding of the card. The design of this card was used in the subsequent chapter to run multiple assays in parallel and determine limits of detection for both the premix and sequential delivery formats.

5.3 Development of a Sequential Assay Protocol

5.3.1 Introduction

Sequential delivery decouples the delivery of analyte and gold conjugate. A wash step between reagents is predicted to ensure a truly step wise delivery of the reagents. In this specific case, a wash step is predicted to aid in the flow through of free analyte that otherwise would be remain upstream of the test line. Without a wash, this free analyte is free to bind with gold conjugate to form an analyte-antibody conjugated to gold nanoparticle complex prior to reaching the test line.

This complex is then able to bind to the capture antibody at the test line. This binding event is identical to what occurs at the test line in the premix delivery format.

Sequential delivery takes four steps (antigen, wash, gold, and wash) while wet premix (antigen/gold and wash) only requires two steps to accomplish. Eliminating the wash step between antigen and gold in the sequential format would shorten the time to results, but may result in high background noise. The minimal number of sequential delivery steps to reduce time to read out without loss of sensitivity due to variable and high nonspecific background was investigated.

A gold conjugate solution at OD 5 was selected; at OD 5, the antibody conjugated to a gold nanoparticle is in excess, and thus not a limiting factor. At lower ODs, the control line is faint and hard to use to create the fiducial mark necessary for the analysis methods. The volumes of the reagents were selected to match closely with the premix volumes for comparison purposes. Both the analyte concentration and OD of the gold conjugate are the same for the premix OD 5 and sequential cases.

5.3.2 Methods

Membrane and Reagent Preparations

Membrane and reagents were prepared as previously outlined in Chapter 4.3.2.

Assay Protocols

Two different wash versus no wash experiments were performed. In the first experiment, 30 µl of sample was added to the sequential with wash membranes. At 7 minutes, a 30 µl TBST wash was added to the sequential with wash membranes and 30 µl of sample added to the sequential

without wash membranes. At 14 minutes, 30 µl of OD 5 gold conjugate was added to all membranes at 15 minutes. At 25 minutes, 40 µl of TBST was added to all membranes and the membranes were scanned at 35 minutes. Four replicates at each of the concentrations 5, 2.5, 0.625, and 0 ng/ml were run. Membranes were run on a simple plastic card with markings etched to expose adhesive for placing the test components. In the second experiment, membranes were run in the card design shown in Figure 16. Four replicates at 5 and 0 ng/ml were run. Due to defects in the membrane, for the no wash set only 3 replicates at 5 ng/ml and for the wash set only 3 replicates at 0 ng/ml were analyzed. A manual protocol outlined in Table 5 was followed.

Table 5. Protocols for sequential delivery without and with wash step after sample.

	Step	**Time**		**Step**	**Time**
Sequential No Wash	10 µl TBST	0	Sequential with Wash	10 µl TBST	0
	30 µl Sample	4		30 µl Sample	4
	Swap Pads	13		Swap Pads	13
	40 µl Gold	14		40 µl TBST	14
	Swap Pads	28		Swap Pads	28
	40 µl TBST	30		40 µl Gold	30
	Scan	44		Swap Pads	44
				40 µl TBST	46
				Scan	60

Image Acquisition and Analysis

A high resolution-scanner (Epson, Nagano, Japan) was used again to acquire image data at 1200 dpi. The images were processed using a custom analysis program (Matlab, Natick, MA). In a graphical display of the image within Matlab, the user selects the center of the control line. A starting location for the center of the test line region of interest (ROI) was set at 375 pixels upstream of the mark and the ROI was swept over a 20 pixel range (along the direction of sample flow) about the starting position. The test line ROI was set at the location of the minimum

average grayscale intensity. A background ROI of the same size (80 pixels by 70 pixels) was defined 140 pixels downstream of the test line ROI and the average grayscale intensity of the background ROI was measured. The normalized signal was defined as the average grayscale intensity in the test line subtracted from the average grayscale intensity in the background.

5.3.3 Results

The necessity of a wash step between the delivery of analyte and delivery of gold conjugate was investigated. The binding pattern at 5 ng/ml in the sequential without wash differs markedly from the binding pattern at 5 ng/ml in the sequential with wash (Figure 25).

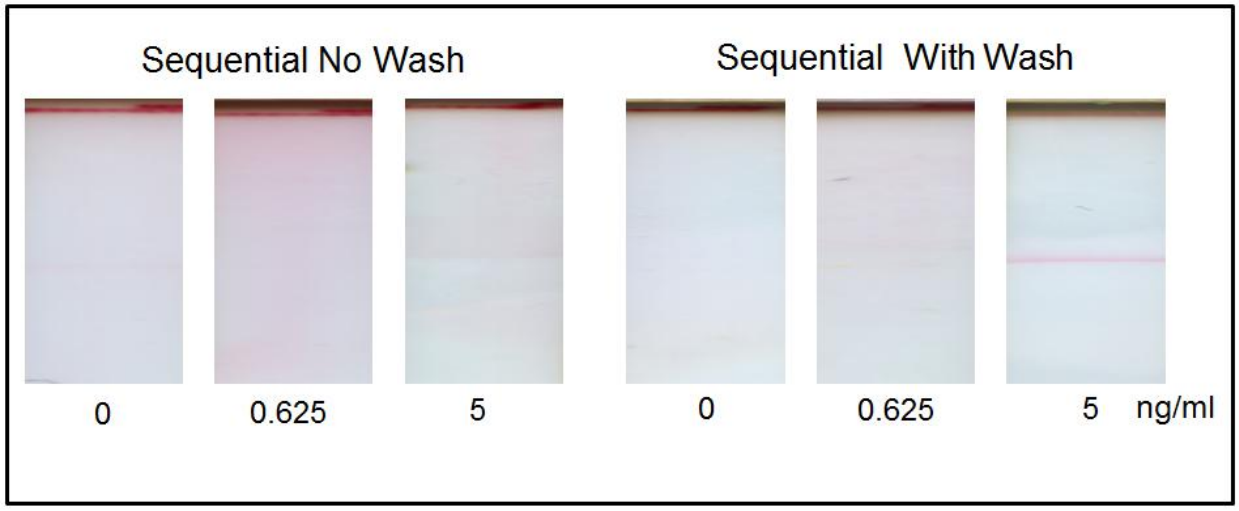

Figure 25. Image series without wash and with wash for the sequential delivery format. There is visible pink background in the without wash membranes.

The pink background seen in the 0.625 ng/ml strip was seen in several other strips in the sequential without wash experimental sets. The source pads between the delivery of the analyte and the delivery of the gold conjugate was not switched.

A subsequent experiment comparing sequential with a wash step and sequential without a wash step between analyte and gold conjugate delivery showed insignificant difference in the binding

pattern and background (Figure 26A). The key difference in this experiment was the source pads were switched after the delivery of analyte and before the delivery of gold conjugate. The normalized signal (Figure 26B) and background signal (Figure 26C) at 5 ng/ml for sequential with wash and sequential without wash was plotted.

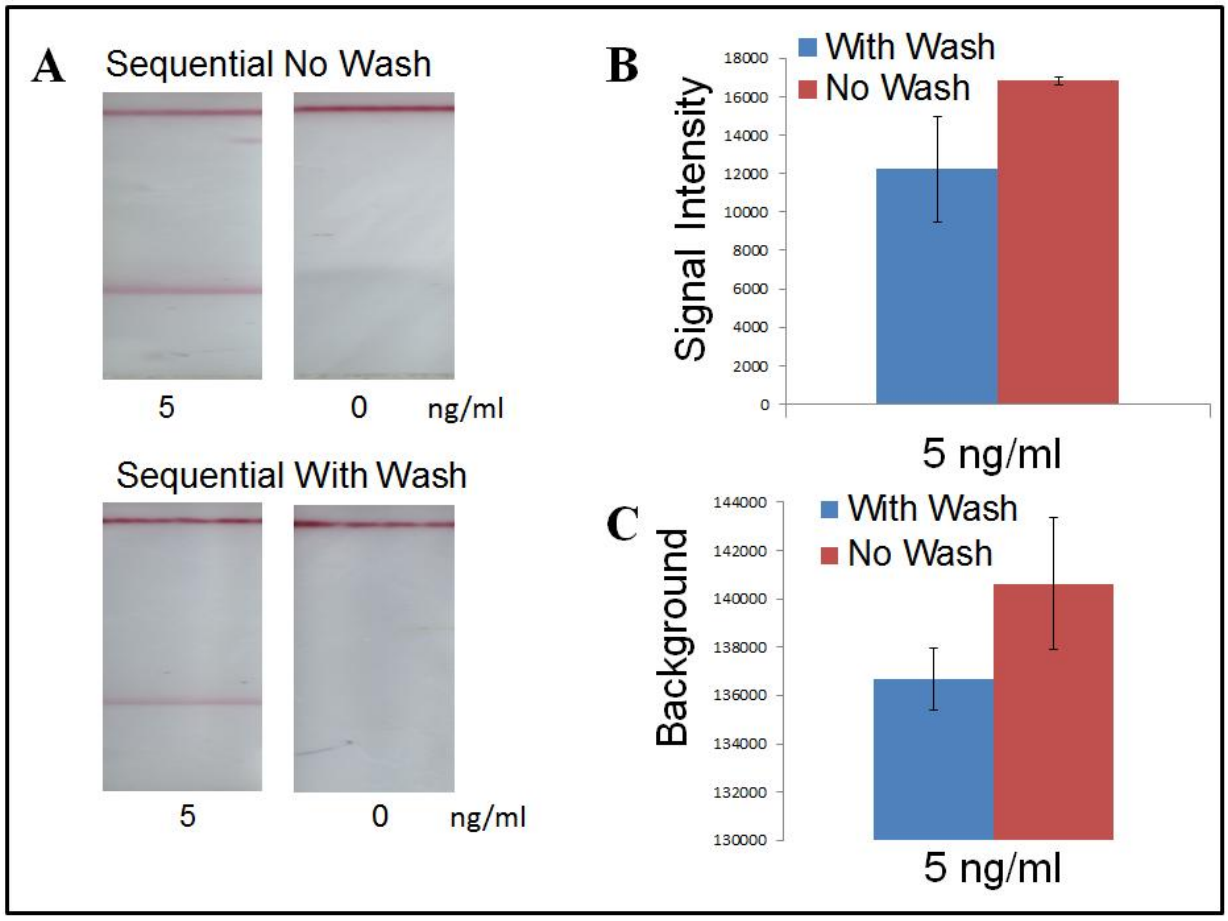

Figure 26. Effect of wash step after sample delivery in the sequential delivery format. (A) Images of membranes run with 5 ng/ml and 0 ng/ml PfHRP2 analyte concentrations without (top) and with a wash step after sample delivery. (B) Plot of average signal intensity with and without the wash step after sample delivery at a PfHRP2 analyte concentration of 5 ng/ml. The average signal intensity is the average of three measurements (without wash) and four measurements (with wash). Error bars represent standard deviation. (C) Plot of the average background signal intensity with and without the wash step after sample delivery at a PfHRP2 concentration of 5 ng/ml. Error bars represent standard deviation.

A two-sample t-test with unequal variances comparing the mean signal intensities with wash and without wash at 5 ng/ml showed a statistically significant difference in means ($p = 0.04$).

5.3.4 Discussion

The first set of experimental results revealed a marked difference in the binding pattern and background in the absence of a wash versus in the presence of the wash. In the case of the binding patterns seen in the absence of a wash step, there is a mixture of uniform binding throughout the entire length of the capture region and high intensity binding localized at the upstream edge of the capture region. The first is characteristic of the premixed delivery of analyte and gold conjugate. The second is characteristic of the sequential delivery of analyte and gold conjugate. In the absence of a wash step, it appeared the delivery of analyte and gold conjugate was not purely step wise. It is predicted that interactions between the analyte and gold conjugate occurred in the source pad prior to reaching the test line region. A small rinse of the source pads between reagents was investigated in Chapter 5.2.3 and found to be ineffective at preventing unwanted reagent interactions outside of the test line region. The more troubling characteristic of the strips without a wash step was the high pink background in several of the strips. This is not attributed to interactions between the gold conjugate and the subsequent wash in the source pads because the source pads were switched between the gold conjugate and final wash step. The source of the pink background was not investigated further.

A second set of experimental results revealed no marked difference in the binding pattern and background in the presence or absence of a wash step between analyte delivery and gold conjugate delivery. The key difference between this experiment and the previous experiment was the source pads were switched after each reagent delivery. The results showed a statistically

significant different in average normalized signal intensity ($p < 0.05$), but visibly no difference in binding pattern or background. This finding suggests that a wash step between analyte delivery and gold conjugate delivery in the sequential format is not necessary as long as detection reagents are introduced via separate source pads. Thus, the sequential delivery format requires 3 steps (analyte, gold conjugate, and a wash). This reduces the time to result of the assay by 16 minutes from 60 minutes down to 44 minutes.

5.3.5 Conclusions

The minimum number of steps in a sequential assay is three (analyte, gold conjugate, and wash). Switching source pads between reagents is advantageous to reduce unwanted interactions outside of the test line region. In most 2DPN designs, reagents are delivered introduced through different source pads. This is ideal given our results showing that interactions occurring in source pads may result in assay variation and background noise.

5.4 Conclusions

With respect to card design, delivering reagents through the same source pad allows unwanted reagent interactions to occur prior to flowing through the test line region. Thus, switching out pads between reagents was determined to be necessary. In most 2DPN designs, reagents are introduced via different source pads. Reagent flow in a fully wetted out membrane was found to have more uniform fluid fronts than a dry membrane previously blocked in a low BSA blocking solution.

Premix and sequential delivery format protocols were determined to minimize the number of steps required without decreasing assay signal and reduce time to result of the overall assay. The

protocols were tested in a card (Figure 20) designed to run four assays simultaneously with reproducible reagent delivery for appropriate reagent delivery times. Table 6 shows the final sequential and premix delivery protocols that were determined.

Table 6. Protocols for premix and sequential delivery formats.

	Step	Time		Step	Time
Premix	10 µl TBST	0	Sequential	10 µl TBST	0
	30 µl Premix Sample	4		30 µl Sample	4
	Swap Pads	13		Swap Pads	13
	40 µl TBST	14		40 µl Gold	14
	Scan	28		Swap Pads	28
				40 µl TBST	30
				Scan	44

The protocols in Table 6 and the card design presented in Figure 20 were used for determining limits of detection for premix and sequential delivery of detection reagents for PfHRP2 protein detection. The sensitivity results for the two delivery formats are presented in the following chapter.

Chapter 6: Sensitivity of Premix and Sequential Delivery Formats

6.1 Objectives

The manual protocols and card design developed in Chapter 5 were used to determine limits of detection for the premix delivery format at two different antibody-conjugated to gold nanoparticle concentrations and the sequential delivery format. Preliminary experimental premix results at OD 0.5 and OD 5 showed an unexpected result. The signal at premix OD 0.5 (lower gold nanoparticle concentration) is higher than the signal at premix OD 5 (higher gold nanoparticle concentration) for an analyte concentration of 20 ng/ml (Figure 27).

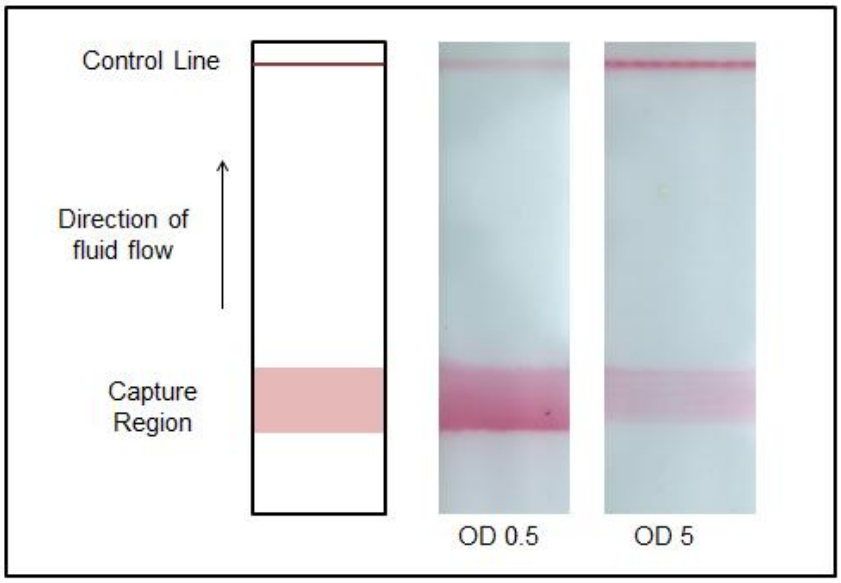

Figure 27. Premix OD 0.5 (middle) and premix OD 5 signal results (right) at 20 ng/ml PfHRP2 analyte concentration. Schematic (left) shows direction of fluid flow and expected locations of the capture region and control line.

The difference in signal at premix OD 0.5 and OD 5 motivated the determination of the limit of detection at both optical densities for the premix delivery format. The limit of detection for the sequential delivery format was determined using a gold conjugate solution at OD 5.

6.2 Sensitivity of Premix and Sequential Delivery Formats

6.2.1 Introduction

Limits of detection for two premix delivery formats with different optical densities of gold conjugate in solution and the sequential delivery format were determined. Manufacturer reported information on the number of gold nanoparticles per mL at varying optical densities (Figure 34 in Appendix C) was used to calculate an approximate antibody concentration. A single gold nanoparticle contains roughly 12 IgG molecules [45]. At OD 5 (5.4×10^{12} IgG molecules per mL), the gold conjugate is in excess, and thus not a limiting factor at the volumes and concentration range of interest. At OD 0.5 (1.08×10^{12} IgG molecules per mL), the gold conjugate is not in excess. The gold conjugate solution will here on be described by optical density unless otherwise specified.

Motivated by the high intensity binding signal at the upstream edge seen in preliminary sequential delivery format data and uniform low intensity binding throughout the capture region in preliminary premix delivery format data, different analysis methods taking into account a 1.48 mm in the direction of flow by 1.69 mm (wide) capture region versus a 0.2 mm in the direction of flow by 1.69 mm (thin) capture region were investigated. Limits of detection results are compared and differences discussed.

6.2.2 Methods

Reagent Preparation

Known concentrations of the recombinant malaria protein PfHRP2 was spiked into fetal bovine serum to serve as a mock sample. TBST (TBS with 0.1 % Tween-20) served as the wash buffer. A premixed solution consisting of five parts gold conjugate at OD 10.2, one part TBS/BSA

solution with 1 % BSA, and four parts mock sample was mixed immediately prior to assay application for the OD 5 data set. Stock gold conjugate at OD 10.2 was diluted in TBS to OD 1. A premixed solution consisting of five parts gold conjugate at OD 1, one part tris buffered saline (TBS) with 1 % BSA, and four parts mock sample was mixed immediately prior to assay application for the OD 0.5 data set. The mock sample concentration used in the premixed solution was adjusted so that the final concentrations of analyte in the premix solution were 0, 0.625, 1.25, 2.5, 5, 10 and 20 ng/ml. For the sequential delivery format, an OD 5 gold conjugate solution was made up of five parts of gold conjugate at OD 10.2, four parts TBS, and one part TBS with 1 % BSA solution. Analyte at concentrations of 5, 2.5, 1.25, 0.625, and 0.3125 were made via serial dilutions.

Membrane and Card Preparation

Membranes and glass fiber pads were prepared as previously described in Chapter 4.3.2. The plastic card housing and base (Figure 20) was cut using a CO_2 laser using the specific cutting parameters outlined in Chapter 3.3. Adhesive layers serve the additional purpose of elevating the membrane surface from touching the surface of the scanner bed, allowing for sequential scans of the same membrane without interference. Overlap between the source pads and membrane and cellulose wicking pad and membrane was kept at 0.5 mm.

Experimental Set-up

All cards were run according to the protocol outlined in Table 6 using the card design shown in Figure 20. All assays were run on the same day using the same stock reagents and batch of patterned membranes. Four identical sets of assays were run with two cards in each set. For the premix delivery format, the first card in each set ran analyte at 20, 10, 5, and 2.5 ng/ml. The

second card in each set ran analyte at 1.25, 0.62, 0 and 0 ng/ml for a total of six non-zero concentrations and three zeros per set. Due to issues with patterning, only three sets of assays for premix OD 5 were included. For the sequential delivery format, the first card in each set ran analyte at 5, 2.5, 1.25, and 0.625 ng/ml. The second card in each set ran analyte at 0.3125, 0, 0, and 0 ng/ml for a total of five non-zero concentrations and three zeros per set.

Image Acquisition and Analysis

A high resolution-scanner (Epson, Nagano, Japan) was used again to acquire image data at 1200 dpi at 28 minutes during the assay. The images were processed using a custom analysis program (Matlab, Natick, MA). The algorithm for defining the region of interest (ROI) is the same as previously described in Chapter 5.3.2. Four average grayscale intensities were extracted per assay: a capture ROI 80 by 70 pixels (wide), a downstream ROI 80 by 70 pixels, a capture ROI 80 by 10 pixels (thin), and a downstream background ROI 80 by 10 pixels. Background ROIs were selected 140 pixels downstream of the test line region. Normalized signal intensity refers to the average grayscale intensity at the test line region subtracted from the average grayscale intensity at the background region. Figure 28 shows the locations of a downstream background region and capture region for both wide capture region and thin capture region.

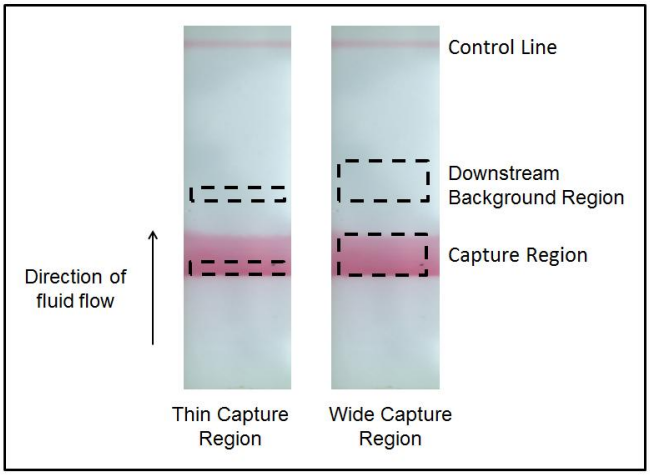

Figure 28. Sample membrane strips showing the locations of the background and capture regions used for analysis. Analysis through a thin capture region (left) and a wide capture region (right) are shown schematically. Schematics are not to scale.

Response curves were created based on the average normalized signal intensities defined as the test line region signal intensity subtracted from the defined background region signal intensity. The limit of detection (LOD) was based on the following formula:

$$LOD = \frac{3 * \sigma}{S}$$

where σ is the standard deviation of the zero concentrations and S is the slope of the response curve. A linear fit through the entire response curve was used to determine the slope. All R^2 values were greater than 0.93. An estimate of the uncertainty in the LOD was calculated using the following formula:

$$\delta LOD = 3\left[\left(\frac{\delta\sigma}{S}\right)^2 + \left(\frac{\sigma * \delta S}{S^2}\right)^2\right]^{1/2}$$

where $\delta\sigma$ is the uncertainty in the standard deviation of the zero concentrations and δS is the standard error of the slope. The formula makes the assumption that the slope error and standard deviation error are independent.

6.2.3 Results

Premix Format

The limits of detection for premix delivery of an OD 5 premix solution and an OD 0.5 premix solution and sequential delivery with an OD 5 gold conjugate solution were determined. Representative images of the concentration series at premix OD 0.5 (Figure 29A) and premix OD 5 (Figure 29B).

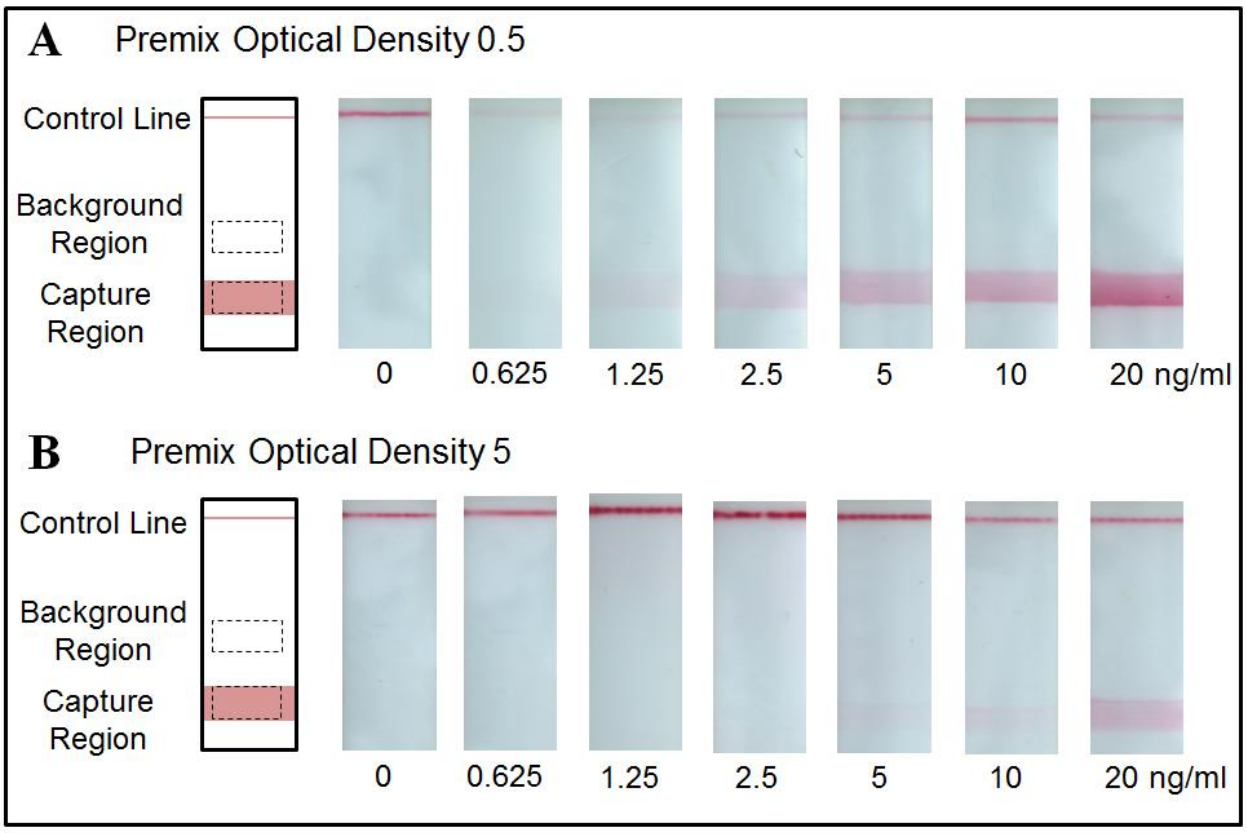

Figure 29. Premix LOD assay results. (A) Image series of the detection region for different concentrations of PfHRP2 analyte for premix at OD 0.5 gold conjugate. (B) Image series of the detection region for different concentrations of PfHRP2 analyte for premix at OD 5 gold conjugate. At the far left is a schematic of the membrane with background, capture, and control line regions labeled. Dashed lines represent regions of analysis across a wide capture region.

For each strip, the normalized signal at the test line was found by subtracting the average grayscale intensity across a defined capture region from the average grayscale intensity at a downstream background region of the same size. The response curves of the two assays, the concentration of PfHRP2 analyte versus the average normalized signal for N=3 or 4 replicates analyzed across a wide capture region was plotted with standard deviations (Figure 30). The response curve is linear across the concentration range tested for the premix format assays. The signal response across the entire concentration series is higher for OD 0.5 premix compared to

OD 5 premix. The limits of detections for premix OD 0.5 and OD 5 were calculated to be 6.48 ± 2.32 ng/ml and 7.71 ± 3.45 ng/ml, respectively when analyzed across a wide, 1.48 mm in the direction flow, capture region. When analyzed over only the first 0.2 mm of where the capture antibody is patterned, the limits of detections for premix OD 0.5 and OD 5 were calculated to be 5.35 ± 1.92 ng/ml and 7.97 ± 3.44 ng/ml, respectively.

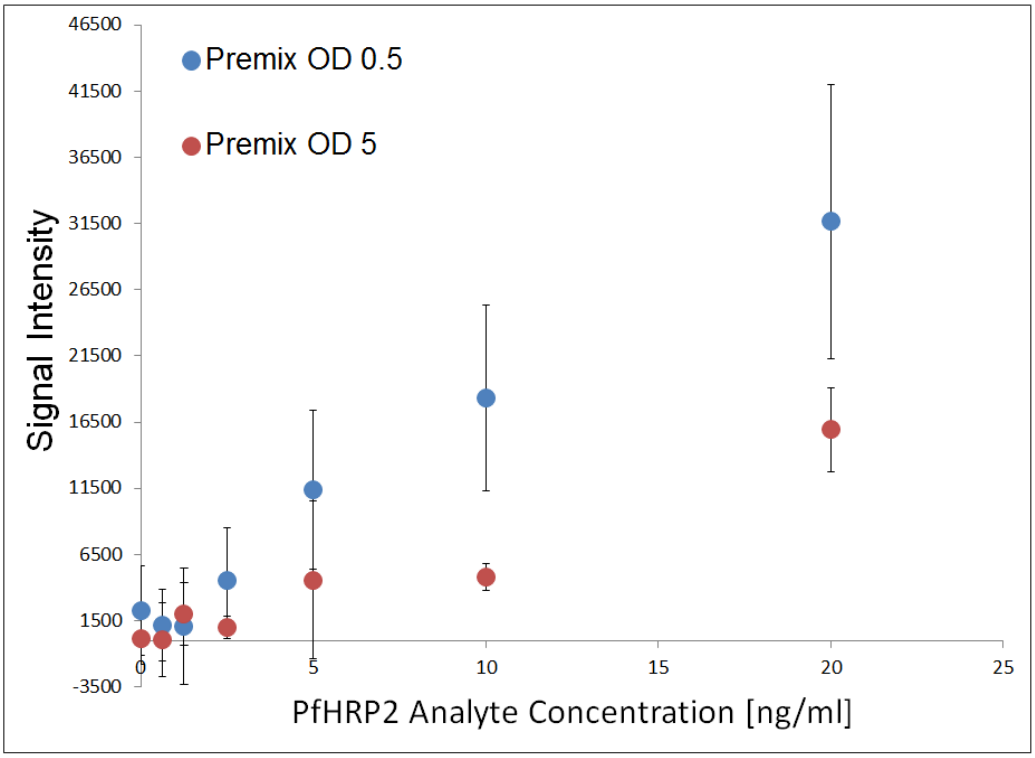

Figure 30. Normalized signal response across a wide capture region for premix OD 5 and premix OD 0.5. Plot of the average signal for each concentration of the LOD results for premix OD 5 and premix OD 0.5. Each data point for premix OD 5 is the average of 3 measurements (with the exception of the 0 ng/ml data point, which is the average of 6 measurements). Each data point for premix OD 0.5 is the average of 4 measurements (with the exception of the 0 ng/ml data point, which is the average of 8 measurements). The error bars represent the standard deviation.

Sequential Delivery Format

The limit of detection for the sequential delivery format was determined. Four replicates at each non-zero concentration and 8 replicates at the zero concentration were run at 5, 2.5, 1.25, 0.625, 0.3125, and 0 ng/ml. A representative image of the concentration series is presented (Figure 31).

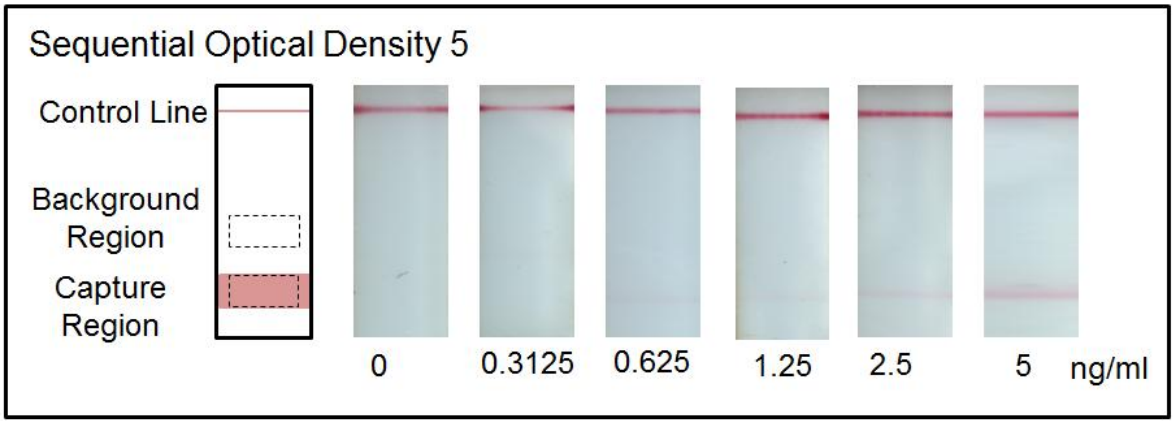

Figure 31. Sequential LOD assay results. Image series of the detection region for different concentrations of PfHRP2 analyte for sequential with OD 5 gold conjugate. At the far left is a schematic of the membrane with background, capture, and control line regions labeled. Dashed lines represent regions of analysis across a wide capture region.

Normalized signals, where the analysis regions were selected as the first 0.2 mm (thin capture region) of where capture antibody was patterned and over a region 1.48 mm in the direction of fluid flow (wide capture region), were calculated. The response curve of the average normalized signal analyzing over the thin capture region was plotted with standard deviations along with the response curve of the average normalized signal analyzing a wide capture region (Figure 32).

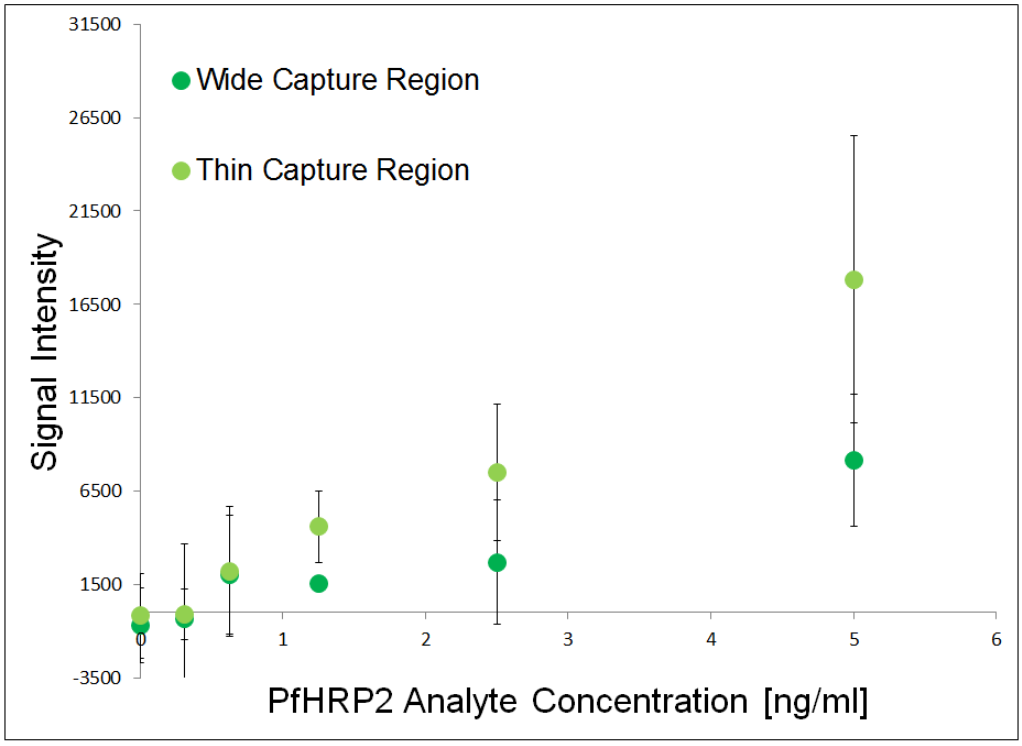

Figure 32. Normalized signal response sequential analyzing a wide capture region and analyzing a thin capture region. Plot of the average signal for each concentration of the LOD results for sequential delivery with OD 5 gold conjugate. Each data point is the average of 4 measurements (with the exception of the 0 ng/ml data point, which is the average of 12 measurements).

The response curve is linear across the concentration range tested. The limit of detection for sequential analyzed across a wide capture region was 3.70 ± 1.18 ng/ml and across a thin capture region was 1.90 ± 0.55 ng/ml. The standard deviations of the zero concentration are similar between analysis of a thin capture region and analysis of a wide capture region, 6788 and 6084, respectively. The slope of the response curve generated from analyzing a thin capture region is about two times the slope of the response curve generated from analyzing a wide capture region.

The response for sequential OD 5 using the thin region of analysis is shown in the plot (Figure 33) with the similarly analyzed data from the premix cases.

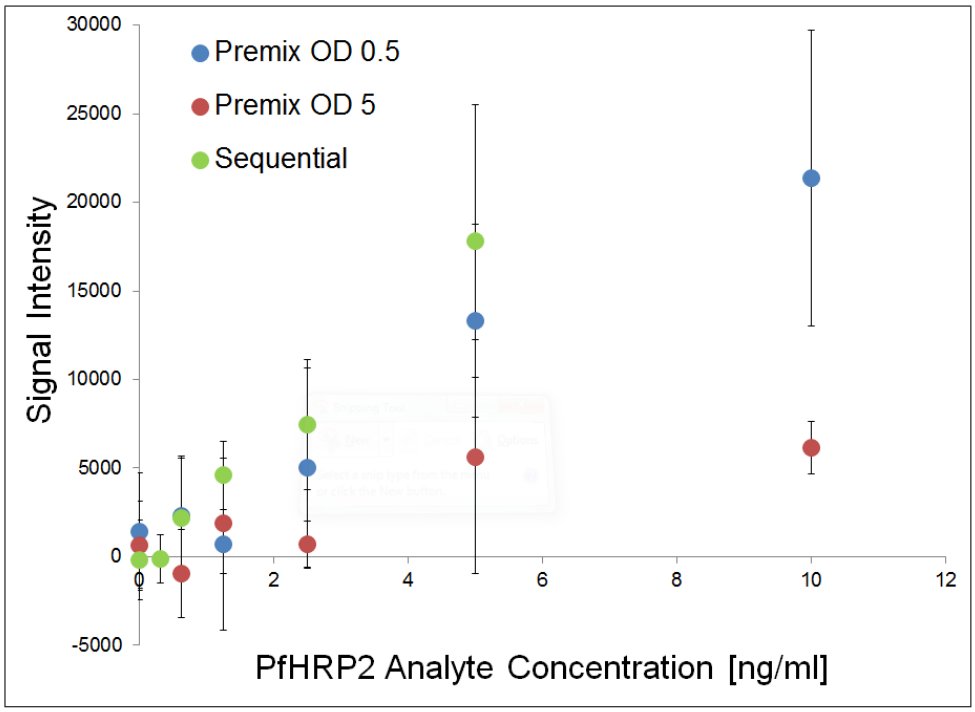

Figure 33. Response curves for premix and sequential delivery formats. Signal intensity refers to the raw signal intensity averaged across the first 2 mm of the upstream portion of the capture region subtracted from a downstream background region. Premix data points are an average of 3 or 4 replicates for non-zero concentrations and 7 or 8 replicates for the zero concentration. Sequential data points are an average of 4 replicates for non-zero concentrations and 12 replicates for the zero concentration. Error bars represent standard deviations.

Table 7 provides a summary of the limit of detection results from a thin capture region during analysis for both the sequential and premix delivery formats.

Table 7. Summary of LOD Results

Delivery Format	Limit of Detection [ng/ml]
Premix OD 0.5	5.35 ± 1.92
Premix OD 5	7.97 ± 3.44
Sequential	1.90 ± 0.55

6.2.4 Discussion

The experimental results were analyzed using multiple analysis methods and the LOD results compared. The normalized signals for premix OD 0.5 was generally higher at the concentrations tested than the normalized signals for premix OD 5. This is particularly evident at the two highest concentrations tested, 20 and 10 ng/ml. One possible explanation for this is the formation of binding complexes consisting of multiple gold nanoparticles. At higher ODs, a PfHRP2 analyte has a higher probability of being bound to multiple gold nanoparticles, making it less likely for the capture IgM at the capture region to capture the PfHRP2 analyte.

The limit of detection values for the premix format results are within the standard LOD error of each other. However, the formula used to calculate the uncertainty in the LOD makes the assumption that the slope error and standard deviation error are independent. This may not be a good assumption for this data set. An alternative method for determining error in LODs, known as the boot strapping method, should be investigated.

A wide capture region appears to offer little advantage over a thin capture region for both the premix and sequential delivery formats. For premix delivery, which produced uniform intensity throughout a wide capture region, there was little difference in average signal for the thick and thin capture regions. This result is expected given that the analysis method chosen is an average of the signal intensity within a specified region.

For the sequential delivery format, there is a two-fold difference in LOD between analyzing only the upstream binding edge and analyzing a wide capture region. The standard deviations of the zeros were consistent regardless of the size of the test line region selected. The main contributor to the LOD difference is the slope of the response curve. The spatial distribution of the binding

is not uniform across the entire length of the test line. Thus, the average grayscale intensity across a wide non-uniform capture region will be lowered due the low binding toward the downstream edge of the capture region. The high binding localized at the upstream edge of the capture patch is predicted to be due to the fast binding kinetics of a free analyte binding to the detection antibody. As the sample solution travels through the capture patch less and less free analyte is available to bind that was not already captured by the capture antibody patterned at the upstream edge. More details on the binding in our system will be discussed in Chapter 6.

Comparing the limit of detection results for premix and sequential analyzing only the upstream binding edge, sequential delivery of the detection reagents has the potential to achieve an approximate four-fold improvement in sensitivity compared to the premix delivery of the same detection reagents. The main disadvantage of sequential delivery is the decoupling of analyte and gold conjugate delivery increases the number of steps in the assay and thus the time to result.

6.2.5 Conclusion

Limits of detection for the premix and sequential delivery formats were determined and summarized in Table 7. Results indicate that the sequential delivery of detection reagents has the potential to achieve around a four-fold improvement in sensitivity over premix delivery of the same detection reagents at the expense of time to result.

Chapter 7: Conclusions

7.1 Overall Conclusions

2DPNs are an inexpensive technology based on the strengths of one-dimensional LFTs. Traditional LFTs make use of a rapid one step delivery of analyte and antibody conjugated to label. 2DPNs allow the delivery of the detection reagents to be decoupled. The porous material components make use of capillary-driven fluid flow. The development of new fluid control tools in the context of 2PDNs enable 2DPNs to carry out multistep chemical processes while still meeting the ASSURED criteria for point-of-care diagnostic tests. Three 2DPN-based amplified assays in the context of malaria detection were demonstrated using three different fluid control tools: paper network geometry, dissolvable sucrose barriers, and cellulose-based delay shunts. These fluid control tools are represent a tool kit for designing 2DPNs with improved user usability and reduced time to result.

The relative affinities for different systems will be different and the resulting sensitivity gains by changing delivery formats are specific for the parameters of that system. In order to understand the benefits that step-wise delivery can have over one step delivery for any system the binding kinetics must be understood. In the case, where the affinity between lone analyte and capture antibody is much greater than the affinity between analyte bound to label and capture antibody, the step wise delivery of analyte and label should be considered during assay design for potential sensitivity gains over the one step delivery of analyte and label.

The potential gains in sensitivity by decoupling the delivery of analyte and antibody conjugated to label was investigated in the context of malaria detection. The sequential delivery format gives high intensity binding at the upstream edge of a long capture region compared to the

uniform binding through the entire capture region seen with the premix delivery format. The distinct binding patterns were predicted to be the result of differences in effective binding constants between the binding pairs. This prediction is supported by experimental results.

With respect to the malaria system presented in this thesis, the limit of detection results using OD 5 gold conjugate for premix delivery of 7.71 ng/ml and sequential delivery of 1.88 ng/ml suggest a potential fourfold gain in sensitivity. Based on the LOD values, for translation into a 2DPN in the context of malaria detection, the sequential delivery format is suggested over the premix delivery format. The sequential delivery format is a promising choice for translation into a 2DPN.

Appendix A: Publications and Presentations

Journal Articles

1. Fu, E.; **Liang, T**.; Houghtaling, J.; Ramachandran, S.; Ramsey, S. A.; Lutz, B.; Yager, P., Enhanced sensitivity of lateral flow tests using a two-dimensional paper network format. *Anal Chem* **2011,** *83* (20), 7941-6.

2. Fu, E.; **Liang, T.**; Spicar-Mihalic, P.; Houghtaling, J.; Ramachandran, S.; Yager, P., Two-dimensional paper network format that enables simple multistep assays for use in low-resource settings in the context of malaria antigen detection. *Anal Chem* **2012,** *84* (10), 4574-9.

3. Lutz, B.; **Liang,T.**; Fu, E.; Ramachandran, S.; Kauffman, P.; Yager, P., Dissolvable fluidic time delays for programming multi-step assays in instrument-free paper diagnostics. *Lab Chip* **2013,** 13, 2840-7.

4. Spicar-Mihalic, P.; Toley, B.; Houghtaling, J.; **Liang, T.**; Yager, P.; Fu, E., CO2 laser cutting and ablative etching for the fabrication of paper-based devices. *Journal of Micromechanics and Microengineering* **2013**, 23

5. Houghtaling, J.; **Liang, T.**; Thiessen, G.; Fu, E., Dissolvable bridges for manipulating fluid volumes in paper networks. *Anal Chem* **2013,** 85(23), 11201-4.

6. Toley, B.; McKenzie, B.; **Liang, T.**; Fu, E., Tunable-Delay shunts for paper microfluidic devices. *Anal Chem* **2013,** 85(23), 11545-52.

7. **Liang T,** et al. Modeling premix and sequential delivery of detection reagents in paper microfluidic assays to improve limit of detection. *In preparation 2014*.

Presentations and Posters

1. **Liang, T;** Fu, E. "Development of a prototype malarial diagnostic device." University of Washington Undergraduate Research Symposium 2012, May 18, 2012: Seattle, WA, USA

2. **Liang, T;** Fu, E. "A novel paper-based diagnostic test with improved sensitivity and usability for low-resource settings." University of Washington Undergraduate Research Symposium 2013, May 17, 2013: Seattle, WA, USA

3. **Liang, T**; Fridley, G; Yager, P; Fu, E. "Investigation of the format-dependent spatial distribution of binding in a malaria antigen assay; implications for higher sensitivity detection." BMES 2014, October 22-25, 2014: San Antonio, TX, USA

Appendix B: References

1. Yager P, Domingo GJ, Gerdes J: **Point-of-care diagnostics for global health**. In: *Annual Review of Biomedical Engineering. Volume 10*, edn. Palo Alto: Annual Reviews; 2008: 107-144.
2. Fauci AS: **Infectious diseases: Considerations for the 21st century**. *Clinical Infectious Diseases* 2001, **32**(5):675-685.
3. **Neglected Tropical Diseases** [http://www.who.int/neglected_diseases/about/en/]
4. Evans JA, Adusei A, Timmann C, May J, Mack D, Agbenyega T, Horstmann RD, Frimpong E: **High mortality of infant bacteraemia clinically indistinguishable from severe malaria**. *Qjm-an International Journal of Medicine* 2004, **97**(9):591-597.
5. **World Mapper: Malaria Deaths** [http://www.worldmapper.org/display.php?selected=230]
6. White NJ: **Antimalarial drug resistance**. *Journal of Clinical Investigation* 2004, **113**(8):1084-1092.
7. Sia SK, Kricka LJ: **Microfluidics and point-of-care testing**. *Lab on a Chip* 2008, **8**(12):1982-1983.
8. Murray CJL, Ortblad KF, Guinovart C, Lim SS, Wolock TM, Roberts DA, Dansereau EA, Graetz N, Barber RM, Brown JC *et al*: **Global, regional, and national incidence and mortality for HIV, tuberculosis, and malaria during 1990-2013: a systematic analysis for the Global Burden of Disease Study 2013**. *Lancet* 2014, **384**(9947):1005-1070.
9. Peeling RW, Holmes KK, Mabey D, Ronald A: **Rapid tests for sexually transmitted infections (STIs): the way forward**. *Sexually Transmitted Infections* 2006, **82**:V1-V6.
10. Moody A: **Rapid diagnostic tests for malaria parasites**. *Clinical Microbiology Reviews* 2002, **15**(1):66-+.
11. Hendriksen ICE, Mtove G, Pedro AJ, Gomes E, Silamut K, Lee SJ, Mwambuli A, Gesase S, Reyburn H, Day NPJ *et al*: **Evaluation of a PfHRP(2) and a pLDH-based Rapid Diagnostic Test for the Diagnosis of Severe Malaria in 2 Populations of African Children**. *Clinical Infectious Diseases* 2011, **52**(9):1100-1107.
12. Murray CK, Gasser RA, Magill AJ, Miller RS: **Update on rapid diagnostic testing for malaria**. *Clinical Microbiology Reviews* 2008, **21**(1):97-+.
13. Chin CD, Laksanasopin T, Cheung YK, Steinmiller D, Linder V, Parsa H, Wang J, Moore H, Rouse R, Umviligihozo G *et al*: **Microfluidics-based diagnostics of infectious diseases in the developing world**. *Nature Medicine* 2011, **17**(8):1015-U1138.
14. Washburn EW: **The dynamics of capillary flow**. *Physical Review* 1921, **17**(3):273-283.
15. Marle CM: **Henry Darcy and fluid flows in porous media**. *Oil & Gas Science and Technology-Revue D Ifp Energies Nouvelles* 2006, **61**(5):599-609.
16. Janeway C, Walport M, Travers P: **Immunobiology: The Immune System in Health and Disease**. New York: Science Publishing; 2005.
17. Linares EM, Kubota LT, Michaelis J, Thalhammer S: **Enhancement of the detection limit for lateral flow immunoassays: Evaluation and comparison of bioconjugates**. *Journal of Immunological Methods* 2012, **375**(1-2):264-270.
18. Kifude CM, Rajasekariah HG, Sullivan DJ, Stewart VA, Angov E, Martin SK, Diggs CL, Waitumbi JN: **Enzyme-linked immunosorbent assay for detection of Plasmodium falciparum histidine-rich protein 2 in blood, plasma, and serum.** *Clin Vaccine Immunol* 2008, **15**(6):1012-1018.
19. Mecklenburg M, Lindbladh C, Li HS, Mosbach K, Danielsson B: **ENZYMATIC AMPLIFICATION OF A FLOW-INJECTED THERMOMETRIC ENZYME-LINKED IMMUNOASSAY FOR HUMAN INSULIN**. *Analytical Biochemistry* 1993, **212**(2):388-393.
20. Engvall E, Jonsson K, Perlmann P: **ENZYME-LINKED IMMUNOSORBENT ASSAY .2. QUANTITATIVE ASSAY OF PROTEIN ANTIGEN, IMMUNOGLOBULIN G, BY MEANS OF ENZYME-**

LABELLED ANTIGEN AND ANTIBODY-COATED TUBES. *Biochimica Et Biophysica Acta* 1971, **251**(3):427-+.

21. Ramachandran S, Fu E, Lutz B, Yager P: **Long-term dry storage of an enzyme-based reagent system for ELISA in point-of-care devices**. *Analyst* 2014, **139**(6):1456-1462.
22. Martinez AW, Phillips ST, Whitesides GM: **Three-dimensional microfluidic devices fabricated in layered paper and tape**. *Proceedings of the National Academy of Sciences of the United States of America* 2008, **105**(50):19606-19611.
23. Martinez AW, Phillips ST, Nie ZH, Cheng CM, Carrilho E, Wiley BJ, Whitesides GM: **Programmable diagnostic devices made from paper and tape**. *Lab on a Chip* 2010, **10**(19):2499-2504.
24. Schilling KM, Lepore AL, Kurian JA, Martinez AW: **Fully Enclosed Microfluidic Paper-Based Analytical Devices**. *Analytical Chemistry* 2012, **84**(3):1579-1585.
25. Schilling KM, Jauregui D, Martinez AW: **Paper and toner three-dimensional fluidic devices: programming fluid flow to improve point-of-care diagnostics**. *Lab on a Chip* 2013, **13**(4):628-631.
26. Lu Y, Shi WW, Qin JH, Lin BC: **Fabrication and Characterization of Paper-Based Microfluidics Prepared in Nitrocellulose Membrane By Wax Printing**. *Analytical Chemistry* 2010, **82**(1):329-335.
27. Abbas A, Brimer A, Slocik JM, Tian LM, Naik RR, Singamaneni S: **Multifunctional Analytical Platform on a Paper Strip: Separation, Preconcentration, and Subattomolar Detection**. *Analytical Chemistry* 2013, **85**(8):3977-3983.
28. Nie JF, Zhang Y, Lin LW, Zhou CB, Li SH, Zhang LM, Li JP: **Low-Cost Fabrication of Paper-Based Microfluidic Devices by One-Step Plotting**. *Analytical Chemistry* 2012, **84**(15):6331-6335.
29. Zhao LC, Yan HT: **A Nitrite Microfluidic Detecting Chip by Fabricating Chlorinated Polyvinyl Chloride Barrier in Filter Paper**. *Acta Chimica Sinica* 2012, **70**(9):1104-1108.
30. Zhou GN, Mao X, Juncker D: **Immunochromatographic Assay on Thread**. *Analytical Chemistry* 2012, **84**(18):7736-7743.
31. Backer M, Raue M, Schusser S, Jeitner C, Breuer L, Wagner P, Poghossian A, Forster A, Mang T, Schoning MJ: **Microfluidic chip with integrated microvalves based on temperature- and pH-responsive hydrogel thin films**. *Physica Status Solidi a-Applications and Materials Science* 2012, **209**(5):839-845.
32. Chen H, Cogswell J, Anagnostopoulos C, Faghri M: **A fluidic diode, valves, and a sequential-loading circuit fabricated on layered paper**. *Lab on a Chip* 2012, **12**(16):2909-2913.
33. Yang XX, Forouzan O, Brown TP, Shevkoplyas SS: **Integrated separation of blood plasma from whole blood for microfluidic paper-based analytical devices**. *Lab on a Chip* 2012, **12**(2):274-280.
34. Apilux A, Ukita Y, Chikae M, Chailapakul O, Takamura Y: **Development of automated paper-based devices for sequential multistep sandwich enzyme-linked immunosorbent assays using inkjet printing**. *Lab on a Chip* 2013, **13**(1):126-135.
35. Gerbers R, Foellscher W, Chen H, Anagnostopoulos C, Faghri M: **A new paper-based platform technology for point-of-care diagnostics**. *Lab on a Chip* 2014, **14**(20):4042-4049.
36. Dharmaraja S, Lafleur L, Brynes S, Kauffman P, Buser J, Toley B, Fu E, Yager P, Lutz B: **Programming paper networks for point of care diagnostics**. *Microfluidics, BioMEMS, and Medical Microsystems XI* 2013, **8615**.
37. Fu E, Kauffman P, Lutz B, Yager P: **Chemical signal amplification in two-dimensional paper networks**. *Sensors and Actuators B-Chemical* 2010, **149**(1):325-328.
38. Fu E, Lutz B, Kauffman P, Yager P: **Controlled reagent transport in disposable 2D paper networks**. *Lab on a Chip* 2010, **10**(7):918-920.

39. Murray CJL, Vos T, Lozano R, Naghavi M, Flaxman AD, Michaud C, Ezzati M, Shibuya K, Salomon JA, Abdalla S *et al*: **Disability-adjusted life years (DALYs) for 291 diseases and injuries in 21 regions, 1990-2010: a systematic analysis for the Global Burden of Disease Study 2010**. *Lancet* 2012, **380**(9859):2197-2223.
40. Shakely D, Elfving K, Aydin-Schmidt B, Msellem MI, Morris U, Omar R, Xu WP, Petzold M, Greenhouse B, Baltzell KA *et al*: **The Usefulness of Rapid Diagnostic Tests in the New Context of Low Malaria Transmission in Zanzibar**. *Plos One* 2013, **8**(9).
41. Lee N, Gatton ML, Pelecanos A, Bubb M, Gonzalez I, Bell D, Cheng Q, McCarthy JS: **Identification of Optimal Epitopes for Plasmodium falciparum Rapid Diagnostic Tests That Target Histidine-Rich Proteins 2 and 3**. *Journal of Clinical Microbiology* 2012, **50**(4):1397-1405.
42. Butterworth AS, Robertson AJ, Ho MF, Gatton ML, McCarthy JS, Trenholme KR: **An improved method for undertaking limiting dilution assays for in vitro cloning of Plasmodium falciparum parasites**. *Malaria Journal* 2011, **10**.
43. Dondorp AM, Desakorn V, Pongtavornpinyo W, Sahassananda D, Silamut K, Chotivanich K, Newton PN, Pitisuttithum P, Smithyman AM, White NJ *et al*: **Estimation of the total parasite biomass in acute falciparum malaria from plasma PfHRP2.** *PLoS Med* 2005, **2**(8):e204.
44. Marquart L, Butterworth A, McCarthy JS, Gatton ML: **Modelling the dynamics of Plasmodium falciparum histidine-rich protein 2 in human malaria to better understand malaria rapid diagnostic test performance.** *Malar J* 2012, **11**:74.
45. Fridley G: **Methods and models to control and predict behavior of two dimensional paper networks for diagnostics**. Seattle, WA: University of Washington; 2014.
46. Cho IH, Seo SM, Paek EH, Paek SH: **Immunogold-silver staining-on-a-chip biosensor based on cross-flow chromatography.** *J Chromatogr B Analyt Technol Biomed Life Sci* 2010, **878**(2):271-277.
47. Holgate CS, Jackson P, Cowen PN, Bird CC: **IMMUNOGOLD SILVER STAINING - NEW METHOD OF IMMUNOSTAINING WITH ENHANCED SENSITIVITY**. *Journal of Histochemistry & Cytochemistry* 1983, **31**(7):938-944.
48. Weipoltshammer K, Schofer C, Almeder M, Wachtler F: **Signal enhancement at the electron microscopic level using Nanogold and gold-based autometallography**. *Histochemistry and Cell Biology* 2000, **114**(6):489-495.
49. Fu E, Liang T, Houghtaling J, Ramachandran S, Ramsey SA, Lutz B, Yager P: **Enhanced Sensitivity of Lateral Flow Tests Using a Two-Dimensional Paper Network Format**. *Analytical Chemistry* 2011, **83**(20):7941-7946.
50. Fu E, Liang T, Spicar-Mihalic P, Houghtaling J, Ramachandran S, Yager P: **Two-Dimensional Paper Network Format That Enables Simple Multistep Assays for Use in Low-Resource Settings in the Context of Malaria Antigen Detection**. *Analytical Chemistry* 2012, **84**(10):4574-4579.
51. Spicar-Mihalic P, Toley B, Houghtaling J, Liang T, Yager P, Fu E: **CO2 laser cutting and ablative etching for the fabrication of paper-based devices**. *Journal of Micromechanics and Microengineering* 2013, **23**(6).
52. Lutz B, Liang T, Fu E, Ramachandran S, Kauffman P, Yager P: **Dissolvable fluidic time delays for programming multi-step assays in instrument-free paper diagnostics**. *Lab on a Chip* 2013, **13**(14):2840-2847.
53. Houghtaling J, Liang T, Thiessen G, Fu E: **Dissolvable Bridges for Manipulating Fluid Volumes in Paper Networks**. *Analytical Chemistry* 2013, **85**(23):11201-11204.
54. Toley BJ, McKenzie B, Liang T, Buser JR, Yager P, Fu E: **Tunable-Delay Shunts for Paper Microfluidic Devices**. *Analytical Chemistry* 2013, **85**(23):11545-11552.
55. Schneider CA, Rasband WS, Eliceiri KW: **NIH Image to ImageJ: 25 years of image analysis**. *Nature Methods* 2012, **9**(7):671-675.

Appendix C: Supporting Materials

Particle Diameter	OD @ 520nm	No. Particles per ml	No. Moles Particle per ml	Molar Particle Concentration (No. moles per L)	Mass of Gold per ml (g)	Moles of Gold per litre
20	1	7.00E+11	1.1624E-12	1.1624E-09	5.66E-05	2.87E-04
20	5	3.50E+12	5.81202E-12	5.81202E-09	2.83E-04	1.44E-03
20	10	7.00E+12	1.1624E-11	1.1624E-08	5.66E-04	2.87E-03
20	15	1.05E+13	1.74361E-11	1.74361E-07	8.49E-04	4.31E-03
20	50	3.50E+13	5.81202E-11	5.81202E-07	2.83E-03	1.44E-02
20	100	7.00E+13	1.1624E-10	5.81202E-05	5.66E-03	2.87E-02
40	1	9.00E+10	1.49452E-13	1.49452E-10	5.82E-05	2.96E-04
40	5	4.50E+11	7.4726E-13	7.4726E-10	2.91E-04	1.48E-03
40	10	9.00E+11	1.49452E-12	1.49452E-09	5.82E-04	2.96E-03
40	15	1.35E+12	2.24178E-12	2.24178E-09	8.73E-04	4.43E-03
40	50	4.50E+12	7.4726E-12	7.4726E-09	2.91E-03	1.48E-02
40	100	9.00E+12	1.49452E-11	1.49452E-08	5.82E-03	2.96E-02
60	1	2.60E+10	4.3175E-14	4.3175E-11	5.68E-05	2.88E-04
60	5	1.30E+11	2.15875E-13	2.15875E-10	2.84E-04	1.44E-03
60	10	2.60E+11	4.3175E-13	4.3175E-10	5.68E-04	2.88E-03
60	15	3.90E+11	6.47625E-13	6.47625E-10	8.51E-04	4.32E-03
60	50	1.30E+12	2.15875E-12	2.15875E-09	2.84E-03	1.44E-02
60	100	2.60E+12	4.3175E-12	4.3175E-09	5.68E-03	2.88E-02
80	1	1.10E+10	1.82664E-14	1.82664E-11	5.69E-05	2.89E-04
80	5	5.50E+10	9.13318E-14	9.13318E-11	2.85E-04	1.44E-03
80	10	1.10E+11	1.82664E-13	1.82664E-10	5.69E-04	2.89E-03
80	15	1.65E+11	2.73995E-13	2.73995E-10	8.54E-04	4.33E-03
80	50	5.50E+11	9.13318E-13	9.13318E-10	2.85E-03	1.44E-02
80	100	1.10E+12	1.82664E-12	1.82664E-09	5.69E-03	2.89E-02

Figure 34. Manufacturer reported information about number of gold nanoparticles per mL at varying OD values. Information from BBInternational, Cardiff, UK.